1

2

3 **Broad-spectrum enzymatic inhibition of CRISPR-Cas12a**

4

5 Gavin J. Knott[1], Brittney W. Thornton[1], Marco J. Lobba[2], Jun-Jie Liu[1], Basem Al-Shayeb[3], Kyle

6 E. Watters[1], and Jennifer A. Doudna[1,2,4-7*]

7

8 [1]Department of Molecular and Cell Biology, University of California, Berkeley, CA, 94720, USA.

9 [2]Department of Chemistry, University of California, Berkeley, CA, 94720, USA.

10 [3]Department of Plant and Microbial Biology, University of California, Berkeley, CA, 94720, USA

11 [4]Molecular Biophysics & Integrated Bioimaging Division, Lawrence Berkeley National

12 Laboratory, Berkeley, USA.

13 [5]Gladstone Institutes, San Francisco, CA, 94158, USA.

14 [6]Howard Hughes Medical Institute, University of California, Berkeley, CA, 94720, USA.

15 [7]Innovative Genomics Institute, University of California, Berkeley, CA, 94720, USA.

16 *Correspondence should be addressed to J.A.D (doudna@berkeley.edu).

17

18   **ABSTRACT**

19   **Cas12a (Cpf1) is a bacterial RNA-guided nuclease used widely for genome editing and**

20   **diagnostic applications. In bacteria, Cas12a enzymes can be inhibited by bacteriophage-**

21   **derived proteins to thwart clustered regularly interspaced short palindromic repeat**

22   **(CRISPR) adaptive immune systems. How these inhibitors disable Cas12a by preventing**

23   **programmed DNA cleavage is unknown. We show that three inhibitors (AcrVA1, AcrVA4**

24   **and AcrVA5) block Cas12a activity using functionally distinct mechanisms, including a**

25   **previously unobserved enzymatic strategy. AcrVA4 and AcrVA5 inhibit double-stranded**

26   **DNA (dsDNA) recognition with AcrVA4 driving Cas12a dimerization. In contrast, AcrVA1**

27   **is a multiple-turnover inhibitor that triggers cleavage of the target recognition sequence of**

28   **the Cas12a-bound guide RNA to irreversibly inactivate the Cas12a complex. These distinct**

29   **mechanisms equip bacteriophage with tools to evade CRISPR-Cas12a and support**

30   **biotechnological applications where multiple-turnover enzymatic inhibition of Cas12a are**

31   **desirable.**

32

33   **INTRODUCTION**

34   Bacteria and archaea can protect themselves against mobile genetic elements and viruses,

35   including bacteriophage, using CRISPR-Cas adaptive immunity[1]. When challenged by a mobile

36   genetic element, bacteria deploy CRISPR-associated (Cas) nucleases guided by an RNA[2,3] to base-

37   pair with the target and mediate target interference to provide immunity against reinfection[3–5].

38   While bacteriophage can undergo rapid mutation and selection to prevent Cas-effector targeting,

39   genetic variation alone is insufficient to escape the potent programmability of bacterial CRISPR-

40   Cas adaptive immunity[6]. To effectively evade CRISPR systems, bacteriophage have evolved

41   protein-based inhibitors – anti-CRISPRs (Acrs)[7] – that inactivate RNA-guided Cas nucleases[8] and

42   enable phage replication[9,10]. In the case of CRISPR-Cas9, such inhibitory Acrs can prevent DNA

43   cutting by blocking dsDNA binding[11–13], promoting Cas9 dimerization[13], or preventing target DNA

2

44 cleavage[13]. Recently, Acrs were discovered that inhibit the activities of the type V-A DNA-

45 targeting CRISPR-Cas12a system[14,15]. These inhibitors targeting Cas12a might be expected to

46 differ in mechanism given that Cas12a has a distinct structure[16,17] and DNA cleavage pathway

47 relative to Cas9[18]. After expression of the CRISPR array and Cas proteins, Cas12a catalyzes

48 precursor CRISPR-RNA (pre-crRNA) processing to form a Cas12a-crRNA complex (or

49 ribonucleoprotein, RNP)[19]. Unlike the commonly used SpCas9, which utilizes two nuclease

50 domains (HNH and RuvC) to cut dsDNA with single-turnover kinetics[20,21], Cas12a possesses a

51 single nuclease domain (RuvC) that is activated upon a crRNA targeting sequence (or spacer)

52 binding to a complementary single-stranded DNA (ssDNA) or dsDNA target molecule[19,22].

53 Furthermore, the Cas12a RuvC domain catalyzes both single-turnover target DNA cutting (*cis*-

54 cleavage) and multiple turnover non-target ssDNA cutting (*trans*-cleavage)[22].

55   To determine the mechanistic basis for Cas12a inhibition, we biochemically assayed

56 inhibition by AcrVA1, AcrVA4, and AcrVA5 on a panel of Cas12a orthologs. While biochemical

57 experiments revealed that no AcrVA was capable of competitively inhibiting the RuvC-nuclease,

58 each AcrVA was able to robustly inhibit dsDNA-targeting and to some extent ssDNA-targeting.

59 Each AcrVA blocked dsDNA binding, but only AcrVA4 dimerized Cas12a and at high

60 concentrations outcompeted dsDNA bound to dLbCas12a. Finally, we show that AcrVA1 triggers

61 multiple turnover endoribonucleolytic cleavage of a Cas12a-bound crRNA to truncate the spacer

62 sequence and permanently inactivate the complex. Together, these data provide the first insights

63 into the mechanisms of AcrVAs, shedding light on the vulnerabilities in Cas12a and the

64 evolutionary arms race between bacteriophage and their host bacteria.

65

66

67   **RESULTS**

68   **AcrVAs do not inhibit all modes of DNA targeting by Cas12a.**

69   Cas12a has a kinetically distinct DNA-cleavage pathway (**Fig 1a**). To determine how

70   AcrVA proteins inhibit Cas12a, we first tested whether AcrVAs competitively inhibit the

71   conserved RuvC nuclease domain. To do this, we determined the Michaelis-Menten constants,

72   Vmax and Km, for the Cas12a RuvC nuclease in the presence of each inhibitor. AcrVA1, AcrVA4

73   and AcrVA5 each reduced the maximum velocity of *trans*-ssDNA cutting by *Lachnospiraceae*

74   *bacterium* (Lb) Cas12a[22] without dramatically affecting the Michaelis-Menten constant for the

75   activated RuvC (**Fig. 1b; Extended data Fig. 1a-d**). These data indicated that AcrVAs were not

76   competitive inhibitors of the RuvC nuclease, but instead somehow depleted the pool of active

77   Cas12a enzyme. We next tested whether AcrVAs could inhibit *cis*-DNA cleavage by Cas12a (**Fig.**

78   **1a**) using radiolabeled DNA substrates and three recombinantly purified Cas12a orthologs that are

79   phylogenetically divergent and/or have been used for genome editing (**Fig. 1c; Extended data Fig.**

80   **2a**). AcrVA1 blocked dsDNA cleavage by all three Cas12a orthologs, whereas AcrVA4 and

81   AcrVA5 were effective against *Moraxella bovoculi* (Mb) Cas12a and LbCas12a but not

82   *Acidaminococcus sp.* (As) Cas12a (**Fig. 1c**), consistent with plasmid cleavage data[14]. The pattern

83   of inhibition was generally the same for Cas12a-mediated ssDNA cleavage but activity was not

84   completely abolished by any inhibitor (**Fig. 1d**; **Extended data Fig. 3a-c**). Collectively, these data

85   indicated that ArcVA1 was a broad-spectrum inhibitor of Cas12a-catalyzed *cis*-DNA cleavage,

86   whereas AcrVA4 and AcrVA5 inhibited *cis*-DNA cleavage catalyzed by MbCas12a and LbCas12a.

87

88   **AcrVAs block dsDNA binding and AcrVA4 dimerizes Cas12a.**

89   We next tested whether AcrVAs affect DNA binding to Cas12a, the rate limiting step of

90   Cas12a-targeting activity[23] (**Fig. 1a**). To test this, we assayed 5'-radiolabelled DNA binding to

91   catalytically dead (dLbCas12a) by electrophoretic mobility shift assays (EMSAs). The dLbCas12a-

92   crRNA complex was formed before the separate addition of each AcrVA and incubation with

93   dsDNA, revealing that AcrVAs abolished dsDNA binding (**Fig. 2a**), while ssDNA binding was

94   perturbed to a lesser extent (**Extended data Fig. 4a, b**). Notably, we observed a slow-mobility

95   species representing the DNA-bound dLbCas12a complex in the presence of AcrVA4 (**Extended**

96   **data Fig. 4c**), hinting at a possible multimeric assembly reminiscent of inhibitor-induced *N.*

97   *meningitidis* (Nme) Cas9 dimerization[13]. To test this possibility, we assessed the solution

98   oligomeric state of each AcrVA and when mixed with LbCas12a-crRNA (**Fig. 2b; Extended data**

99   **Fig; 5a, b**). While AcrVA1 and AcrVA5 appeared monomeric (**Extended data Fig. 5a, b**),

100 AcrVA4 appeared dimeric prior to complexing with Cas12a (**Fig. 2b**). Although neither AcrVA1

101 nor AcrVA5 triggered a substantial change in estimated molecular weight when complexed with

102 LbCas12a-crRNA (**Extended data Fig. 5a, b**), mixing AcrVA4 with LbCas12a-crRNA produced

103 two higher molecular weight species (**Fig. 2b**). Using light scattering, we estimated the mass of

104 these species to be 349 kDa and 214 kDa respectively, consistent with a dimeric LbCas12a protein-

105 crRNA-AcrVA4 complex and a monomeric LbCas12a-crRNA bound to a dimer of AcrVA4. To

106 directly visualize the dimerization of LbCas12a-crRNA with AcrVA4, we analyzed gel filtration

107 purified fractions by negative stain electron microscopy, revealing a distribution of particles

108 including a symmetrical complex of LbCas12a-crRNA dimers (**Fig. 2c**; **Extended data Fig. 5c**).

109 Taken together, these results demonstrate that AcrVAs block dsDNA binding to Cas12a and that

110 the mechanism for AcrVA4 involves dimerization of the LbCas12a-crRNA complex.

111

112 **AcrVA4 can dislodge dsDNA bound to dCas12a.**

113   We next wondered if any AcrVA was capable of disrupting dsDNA-bound complexes of

114 Cas12a-crRNA, a mechanism that may have evolved to disable an activated and *trans*-cleaving

115 Cas12a (**Fig. 1a**). To test this possibility, we formed a ternary complex of dLbCas12a-crRNA

116 bound to radiolabeled dsDNA to which was added a titration series of excess AcrVA1, AcrVA4,

117 AcrVA5, or unlabeled dsDNA and visualized by EMSA. At high concentrations, AcrVA4 triggered

118 the release of dsDNA bound to Cas12a, whereas little dsDNA release occurred in the presence of

119   AcrVA1, AcrVA5, or unlabeled dsDNA competitor (**Fig. 3a; Extended data Fig. 6a**). In contrast,

120   a stoichiometric excess of any AcrVA or ssDNA competitor had no effect on dLbCas12a-crRNA

121   bound to radiolabeled ssDNA (**Extended data Fig. 6b**). These data suggest that at high

122   concentrations AcrVA4 can dislodge dsDNA after it has formed an R-loop interaction with Cas12a.

123   Depletion or addition of ATP had no effect on dsDNA displacement from LbCas12a-crRNA

124   complexes by AcrVA4, suggesting an ATP-independent process (**Extended data Fig. 6c**).

125   AcrVA4 did not trigger release of ssDNA bound to dLbCas12a-crRNA, suggesting that the non-

126   target strand (NTS) of the DNA (the strand not base-paired to the crRNA) might be required to

127   drive re-annealing with the target strand (TS). In support of this possibility, addition of the NTS

128   ssDNA molecule to the dLbCas12a-crRNA-TS DNA complex led to TS DNA displacement in the

129   presence of AcrVA4; a non-complementary ssDNA used in a similar experiment had no effect

130   (**Extended data Fig. 7a**). Consistent with TS DNA release requiring base pairing to a

131   complementary NTS strand, AcrVA4 was unable to drive DNA release from dLbCas12a-crRNA

132   bound to a dsDNA substrate containing mismatched nucleotides along all or some of the 20-nt NTS

133   (**Extended data Fig. 7b**, **c**).

134   The preceding experiments were conducted using catalytically inactive Cas12a, which

135   prevents cutting of bound DNA and hence remains associated with an intact dsDNA molecule.

136   Given that catalytically active Cas12a would cut and release the PAM distal dsDNA fragment after

137   the formation of an R-loop interaction[24], we reasoned that this release might prevent AcrVA4 from

138   displacing the PAM proximal dsDNA bound to the crRNA (**Fig. 1a**). To test this possibility, we

139   incubated wild-type LbCas12a-crRNA with a dsDNA substrate, followed by addition of AcrVA4

140   and analysis of the resulting samples by EMSA (**Fig. 3b**). In contrast to dLbCas12a (**Fig. 3a;**

141   **Extended data Fig. 7d**), AcrVA4 had no effect on DNA bound by wild-type LbCas12a (**Fig. 3b**).

142   These data demonstrate that AcrVA4 can dislodge dsDNA bound to catalytically dead but not

143   active Cas12a, presumably due to a shift in binding equilibrium that favors DNA strand re-

144   annealing.

145

146 **AcrVA1 triggers endoribonucleolytic truncation of a Cas12a-bound crRNA**

147   We next explored whether AcrVA1 or AcrVA5 prevent target DNA binding by disruption

148 of the Cas12a-crRNA complex (**Fig. 1a**). To test this possibility, we incubated Cas12a with each

149 AcrVA individually before adding radiolabeled RNA to probe crRNA integrity, the efficacy of pre-

150 crRNA processing, and the affinity of Cas12a for mature crRNA. We were surprised to observe

151 that AcrVA1 induced rapid 3'-end truncation of both mature and pre-crRNA in the presence of

152 Cas12a (**Fig. 4a; Extended data Fig. 8a**). In these experiments, neither binding to mature crRNA

153 or pre-crRNA processing were affected (**Fig. 4b; Extended data Fig. 8a**). Notably, AcrVA1 had

154 no effect on the integrity of mature or pre-crRNA in the absence of Cas12a, and neither AcrVA4

155 nor AcrVA5 had any effect on crRNA in the absence or the presence of Cas12a (**Fig. 4a, b;**

156 **Extended data Fig. 8a, b**). Pre-assembly of Cas12a and crRNA forms the Cas12a-crRNA complex

157 which was also susceptible to AcrVA1-mediated crRNA 3'-truncation (**Extended data Fig. 8b**).

158 However, assembly of an activated Cas12a-crRNA complex with the addition of complementary

159 ssDNA or dsDNA prevented AcrVA1-mediated crRNA truncation (**Extended data Fig. 8c**).

160 Furthermore, AcrVA1-mediated crRNA truncation was specific for a crRNA bound by Cas12a

161 regardless of spacer sequence (**Extended data Fig. 9a**) or lengths that support Cas12a DNA-

162 targeting[19,22] (**Extended data Fig. 9b**), and without any detectable non-specific ribonuclease

163 activity (**Extended data Fig. 9c**). Taken together, the above data indicate that AcrVA1 triggers

164 crRNA truncation on an assembled Cas12a-crRNA complex.

165   Interestingly, AcrVA1 is not predicted to be a nuclease[14,15], nor does it have detectable

166 RNA cleavage activity in the absence of a Cas12a-crRNA complex (**Fig. 4a; Extended data Fig.**

167 **9a-c**). To assess the mechanism of AcrVA1-mediated RNase activity, we mapped the scissile

168 phosphates at positions five to eight within the crRNA spacer, with some plasticity in position

169 dependent on the Cas12a ortholog (**Fig. 4c; Extended data Fig. 9d**). The activity is that of an

170 endoribonuclease where catalysis generates an intact 3'-fragment of the crRNA that is released by

171 Cas12a after AcrVA1-triggered truncation (**Extended data Fig. 9e-f**). To identify the nuclease

172 center responsible for crRNA truncation we targeted Cas12a's nucleases for mutagenesis, the RuvC

173 or pre-crRNA processing nuclease, and observed that mutation of either did not prevent AcrVA1-

174 triggered spacer truncation (**Fig. 4c; Extended data Fig. 9d**). We next assayed the metal-

175 dependency of the nuclease by supplementing with $MgCl_2$ or EDTA and observed that AcrVA1-

176 triggered spacer truncation was not dependent on divalent cations (**Extended Data Fig. 9g**).

177 Consistent with this, we determined the end-group chemistry of the 5'-radiolabeled crRNA

178 fragment with T4 polynucleotide kinase (PNK) treatment which resulted in an upward shift in

179 polyacrylamide gel migration, indicating that the 5'-fragment generated has a 3'-phosphate at its

180 terminus (**Fig. 4d**). Taken together, these data demonstrate that AcrVA1 triggers metal-ion

181 independent endoribonucleolytic cleavage of the targeting portion of the crRNA which then

182 dissociates to render the complex rudderless with respect to DNA targeting (**Fig. 4e**).

183

184 **AcrVA1 is a multiple-turnover inhibitor and competes with AcrVA5**

185   AcrVA1 stands out among the known Cas12a and Cas9 inhibitors as a highly effective and

186 broad-spectrum inhibitor of RNA-guided dsDNA targeting by Cas12a[14]. Given its unique

187 enzymatic activity, we wondered if the potency of AcrVA1 inhibition might be attributed to

188 multiple-turnover kinetics. To test this, we incubated a range of AcrVA1 concentrations with

189 Cas12a-crRNA complexes and in all cases observed ~95% of crRNAs truncated, even at sub-

190 stoichiometric concentrations of AcrVA1 (**Fig. 5a**). Thus, AcrVA1 activity is multiple-turnover

191 where cleavage of a crRNA will permanently inactivate Cas12a-crRNA complexes through a mode

192 of inhibition not previously observed for any anti-CRISPR protein. However, we earlier

193 demonstrated that AcrVA1 was not a robust inhibitor of ssDNA targeting by Cas12a (**Fig. 1d;**

194 **Extended Data Fig. 3**) which is at odds with the observed nuclease activity on the crRNA (**Fig.**

195 **4a; Fig. 5a**). We wondered if the 5'- or 3'-fragments of the crRNA, together or separately, might

196 still be sufficient for ssDNA-targeting. To test this, we prepared RNA fragments that mimic

197   products of AcrVA1 activity and assayed ssDNA-targeting by LbCas12a. Remarkably, LbCas12a

198   cleaved ssDNA in the presence of both the 5'- and 3'-fragments (**Extended Data Fig. 10c**),

199   suggesting that the ssDNA-targets can be recruited to Cas12a with a two-component crRNA. Taken

200   together, our data demonstrate that AcrVA1 triggers crRNA truncation and release of the 3'-

201   fragment from Cas12a which can hybridize with a target ssDNA to activate *cis* and *trans*-ssDNA

202   cleavage by Cas12a.

203   The ability of AcrVA1 to inhibit diverse Cas12a orthologs (**Fig. 1c**) suggested that it might

204   exploit an evolutionarily conserved domain of Cas12a. To determine domains required for

205   AcrVA1-triggered spacer truncation, we generated truncations that still allowed for crRNA binding

206   and pre-crRNA processing. Removal of either the PAM-interacting domain (PID) or both

207   recognition (REC) domains generated stable constructs that maintained near wild-type mature

208   crRNA binding affinity or pre-crRNA processing (**Extended data Fig. 10b, c**). However, only in

209   the absence of the PID was AcrVA1-triggered crRNA truncation prevented (**Fig. 5b**). Finally, we

210   wondered if either AcrVA4 or AcrVA5 might compete with the AcrVA1-triggered spacer

211   truncation activity. To test this, we first incubated an LbCas12a RNP with either AcrVA4 or

212   AcrVA5 before adding AcrVA1 and found that AcrVA5 reduced the rate of AcrVA1-triggered

213   crRNA truncation (**Fig. 5c**), suggesting that AcrVA5 does compete with the spacer truncation

214   activity of AcrVA1.

215

216   **DISCUSSION**

217   CRISPR-Cas12a are RNA-guided DNA-targeting nucleases with robust *cis*-cleavage and

218   ssDNA *trans*-cleavage, activities that have led to their rapid implementation as tools for genome

219   engineering and diagnostics[25]. In this work, we present the first mechanistic insights into type V-

220   A bacteriophage-derived anti-CRISPRs elucidating the distinct mechanisms leveraged to inactivate

221   Cas12a (**Fig. 6**). We found that AcrVA1, AcrVA4, and AcrVA5 robustly inhibited Cas12a dsDNA

222   targeting, not unlike inhibitors that evolved to target Cas9[26].

223   AcrVA1 provides a uniquely potent mechanism for evading CRISPR adaptive immunity

224   by triggering crRNA truncation with multiple turnover kinetics to rapidly and permanently

225   inactivate the Cas12a surveillance complex. We demonstrated that the nuclease activity is entirely

226   dependent on the presence of a Cas12a-crRNA complex and AcrVA1, but our data do not describe

227   the identity of the component bearing the catalytic center for the observed nuclease activity. It is

228   likely that AcrVA1 is an RNase, however we could not detect any RNase activity on free crRNA

229   or *trans*-ssRNA substrates, suggesting that its activity is allosterically activated by binding to a

230   Cas12a-crRNA complex or that Cas12a harbors the nuclease domain or a part thereof. AcrVA1 has

231   a broad spectrum of inhibition, disabling divergent Cas12a nucleases *in vitro* and in mammalian

232   cell editing[14] potentially exploiting the broadly conserved PAM interacting domain for direct

233   access to the pre-ordered seed of the crRNA[27]. Interestingly, AcrVA1 displayed less robust

234   inhibition of Cas12a ssDNA-targeting, a potential artefact of working *in vitro* as the cleaved 3'-

235   crRNA fragments can readily associate with ssDNA and be recruited back to Cas12a for activation.

236   In the bacterial host, it is likely that cleavage of the crRNA creates an ineffective two-component

237   system. However, further experiments are required to determine if AcrVA1 provides a selective

238   advantage to ssDNA plasmids or ssDNA phage. It was recently shown that bacteriophage cooperate

239   to immunocompromise bacterial hosts, delivering Acrs iteratively to gradually overcome CRISPR-

240   Cas immunity[10,28]. In light of these observations, bacteriophage encoding AcrVA1 may be the most

241   effective in supporting populations of phage lacking Acrs given its multiple turnover kinetics even

242   with the recent data suggesting that Cas12a endonuclease activity can be reset[29]. The unique

243   mechanism for AcrVA1-mediated CRISPR-Cas12a inhibition may lend itself to potent control of

244   Cas12a in gene editing applications where it is desirable to block DNA targeting or limit

245   unintended editing events.

246   We also found that AcrVA4 blocks dsDNA binding in addition to driving dimerization of

247   Cas12a-crRNA complexes. This mechanism has also been described for AcrIIC3 which targets

248   NmeCas9[13]. While mechanistically and structurally divergent, Cas9 and Cas12a are susceptible to

249 a convergent mechanism of inhibition suggesting that higher order assembly of Cas nucleases and

250 the associated inhibitors offers an as yet unclear benefit to bacteriophage. AcrVA4 was also able

251 to disrupt a dLbCas12a-crRNA complex stably associated with dsDNA, an activity that required

252 high concentrations of the inhibitor. The disruption of dLbCas12a dsDNA bound states may have

253 applicability in dLbCas12a-mediated transcriptional control applications, however further

254 experiments are required to establish the off-rate for dsDNA in the presence of AcrVA4.

255 Furthermore, while it is interesting to consider that AcrVA4 may shift the equilibrium in favor of

256 dsDNA dissociation, this mode of action is unlikely to have biological significance given that wild-

257 type Cas12a rapidly catalyzes DNA-cleavage once an R-loop is formed[29,30].

258   Finally, we demonstrated that AcrVA5 robustly inhibited Cas12a dsDNA-targeting activity

259 by preventing dsDNA binding. Given that AcrVA5 competed with AcrVA1 and that AcrVA1

260 activity is dependent on the PID, we speculate that AcrVA5 may directly exploit the PID to block

261 PAM recognition on dsDNA substrates. If true, this raises the possibility that AcrVA5 might be

262 leveraged as a tool to block *in vivo* dsDNA targeting by Cas12a in order to exclusively select for

263 ssDNA targeting. Furthermore, this panel of AcrVA inhibitors are more potent inhibitors of

264 dsDNA-targeting than ssDNA-targeting by Cas12a which may reflect an evolutionary pressure

265 from dsDNA phage in the hosts microbial community. Taken together, these mechanistic insights

266 reveal vulnerabilities in the modes of Cas12a targeting and provide scope for greater control of

267 Cas12a in applications.

268

269   **METHODS**

270   **Phylogenetic analysis**

271   A multiple sequence alignment of the Cas12 proteins[19,30,31] was generated using MAFFT L-INS-

272   i[32] and a maximum-likelihood phylogenetic tree was constructed using RAxML[33] with

273   PROTGAMMALG as the substitution model and 100 bootstrap samplings. The tree was visualized

274   using iTOL v3[34] to highlight the phylogeny of Cas12a with Cas12b-e as a collapsed outgroup.

275

276   **Protein expression and purification**

277   Plasmids encoding *Moraxella bovoculi* (33362) Cas12a, *Lachnospiraceae bacterium* (ND2006)

278   Cas12a, *Acidaminococcus sp.* (BV3L6) Cas12a, AcrVA1, AcrVA4, and AcrVA5 were generated

279   from a custom pET-based expression vector as described previously[14]. Cas12a point mutations and

280   truncations were introduced by either around-the-horn PCR or Gibson Assembly verified by DNA

281   sequencing. Proteins were purified as described previously[14]. Briefly, *E. coli* Rosetta 2 (DE3)

282   containing Cas12a or AcrVA expression plasmids were grown in Lysogeny Broth overnight with

283   ampicillin (100 μg mL^{-1}). Overnight cultures were sub-cultured in Terrific Broth to an OD_{600} of

284   0.6-0.8, after which the cultures were cooled on ice for 15 min before induction with 0.5 mM IPTG

285   and incubated overnight at 16°C for 16 hrs. Cells were harvested by centrifugation and resuspended

286   in wash buffer (20 mM Tris-Cl, (pH 7.5), 500 mM NaCl, 1 mM TCEP, 5% (v/v) glycerol)

287   supplemented with 0.5 mM PMSF and cOmplete protease inhibitor (Roche), lysed by sonication,

288   and purified over Ni-NTA Superflow resin (Qiagen) in wash buffer supplemented with either 10

289   mM imidazole (wash) or 300 mM imidazole (elution). Eluted proteins were digested overnight

290   with TEV protease at 4°C in a Slide-A-Lyzer (10 kDa MWCO, Thermofisher) against dialysis

291   buffer (20 mM Tris-Cl (pH 7.5), 125 mM NaCl, 1 mM TCEP, 5% (v/v) glycerol). Digested proteins

292   were loaded onto an MBP-Trap (GE Healthcare) upstream of a Heparin Hi-Trap (GE Healthcare,

293   Cas12a) or a Hi-Trap Q (GE Healthcare, AcrVA) and eluted over a salt gradient (20 mM Tris-Cl,

294   (pH 7.5), 1 mM TCEP, 5% (v/v) glycerol, 125 mM – 1 M KCl). The eluted protein was

295   concentrated before injection to a Superdex 200 10/300 Increase (GE Healthcare) developed in 20

296   mM HEPES-K (pH 7.5), 200 mM KCl, 1 mM TCEP, 5% (v/v) glycerol). Purified proteins were

297   concentrated and snap frozen in LN_2 for storage at -80°C. The purity and integrity of proteins used

298   in this study were assessed by SDS-PAGE (Coomassie blue staining) (**Extended data Fig. 2b**).

299

300   **RNA and DNA preparation**

301   RNA used in this study were ordered from Integrated DNA Technologies (IDT) (**Extended data**

302   **Table 1**). RNA substrates were purified by gel extraction from 12% (v/v) urea-denaturing PAGE

303   (0.5X TBE) and ethanol precipitation as described previously[35]. All DNA substrates were

304   synthesized by IDT and purified as described above. Radiolabeled RNA substrates were prepared

305   by 5'-end-labeling with T4 PNK (NEB) in the presence of gamma ^{32}P-ATP. For 3'-end-labeled

306   substrates, the crRNA was labeled with T4 RNA Ligase 1 (NEB) in the presence of ^{32}P-PcP.

307   Radiolabeled DNA substrates were prepared by 5'-end-labeling with T4 PNK (NEB) in the

308   presence of gamma ^{32}P-ATP. For dsDNA substrates, non-target strand or target-strand was first 5'-

309   end-labeled before annealing a 1.2-fold molar excess of the complementary strand at 95°C for 3

310   min in 1X hybridization buffer (20 mM Tris-Cl, pH 7.5, 150 mM KCl, 5 mM $MgCl_2$, 1 mM DTT)

311   followed by slow-cooling to room temperature.

312

313   **DNase-Alert *trans*-cleavage assays**

314   For Michaelis-Menten kinetics in the presence or absence of AcrVA, 0.1 nM of pre-assembled and

315   activated LbCas12a-crRNA-activator holoenzyme was prepared by complexing 5 nM Cas12a and

316   6.25 nM crRNA (15 min at 37°C) with 25-50 nM AcrVA (30 min at 37°C) and 0.1 nM DNA

317   activator (15 min at 37°C) in 1X *trans*-cleavage buffer (20 mM HEPES-K (pH 7.5), 100 mM KCl,

318   5 mM $MgCl_2$, 5% (v/v) glycerol, 1 mM DTT, 50 µg/mL heparin). Reactions were initiated with

319   0.001, 0.01, 0.1, 0.25, 0.5, 1, or 2 µM of DNase-Alert™ substrate (IDT). Reactions were incubated

320   in a fluorescence plate reader (BioTek) for 30 min at 37°C with fluorescence measurements taken

321 every 20 sec (λ_{ex}: 535 nm; λ_{em}: 595 nm). The initial velocity (V_0) was calculated by fitting to a

322 linear regression and plotted against the substrate concentration to determine the Michaelis-Menten

323 constants (Prism7, GraphPad), according to $Y = (V_{max} \times X)/(K_m + X)$, where X is the substrate

324 concentration and Y is the initial velocity ($n = 3$ independent measurements).

325

326 **Radiolabeled DNA cleavage assays**

327 Cas12a-mediated DNA-cleavage assays were carried out in 1X cleavage buffer (20 mM Tris-Cl

328 pH (7.8), 150 mM KCl, 5 mM $MgCl_2$, 1% (v/v) glycerol, and 2 mM DTT). Radiolabeled DNA-

329 cleavage assays consisted of Cas12a, crRNA, and ^{32}P-labeled DNA substrates in the presence or

330 absence of AcrVA at 30 nM, 36 nM, 1 nM, and 300 nM, respectively. The RNP was formed at

331 37°C for 15 minutes before addition of AcrVA (unless otherwise indicated) and incubated at 37°C

332 for 30 minutes. Reactions were initiated with the addition of target DNA at 37°C and timepoints

333 (1, 2, 5, 15, 60 min) quenched in 1.5X formamide loading buffer (final concentration 45% (v/v)

334 formamide, 15 mM EDTA, 0.1% (w/v) SDS, 200 μg mL^{-1} Heparin, and 0.25% (w/v) bromophenol

335 blue) for 3 min at 95°C. Samples were resolved by 12% (v/v) urea-denaturing PAGE (0.5X TBE)

336 and visualized by phosphoroimaging (Amersham Typhoon, GE Healthcare). The percentage

337 cleavage was calculated as a ratio of the intensity of the product band relative to the total intensity

338 of both the product and uncleaved DNA normalized to the background within each measured

339 substrate in ImageQuant TL Software (GE Healthcare). Apparent rates were calculated by a fit to

340 a single exponential decay (Prism7, GraphPad). The rates with their associated standard deviations

341 are included in the figure legends ($n = 3$ independent measurements).

342

343 **Radiolabeled crRNA cleavage assays**

344 crRNA-cleavage assays were carried out in 1X cleavage buffer. Radiolabeled crRNA-cleavage

345 assays consisted of Cas12a, and ^{32}P-labeled RNA substrates in the presence or absence of AcrVA

346 at 50 nM, 1 nM, and 500 nM, respectively. Complexing was carried out by incubating Cas12a and

347 AcrVA or ^{32}P-labeled crRNA substrates at 37°C for 30 min before initiating the reaction with the

348 addition of AcrVA or ^{32}P-labeled RNA substrates. Reaction timepoints (1, 2, 5, 15, 60 min) were

349 quenched in 1.5X formamide loading buffer for 3 min at 95°C. Samples were resolved by 12%

350 (v/v) urea-denaturing PAGE (0.5X TBE), visualized by phosphoroimaging (Amersham Typhoon,

351 GE Healthcare), and quantified with ImageQuant TL Software (GE Healthcare). Where

352 appropriate, apparent rates were calculated by a fit to a single exponential decay (Prism7,

353 GraphPad), and the calculated rates with their associated standard deviations are included in the

354 figure legends ($n = 3$ independent measurements). For substrate turnover experiments, 120 nM of

355 Cas12a was complexed with 100 nM of mature crRNA and incubated with 10, 25, 50, 100, 150, or

356 200 nM AcrVA1 at 37°C for 60 min before quenching in 1.5X formamide loading buffer for 3 min

357 at 90°C. Samples were resolved by 12% (v/v) urea-denaturing PAGE (0.5X TBE), visualized with

358 SYBR Gold (Invitrogen) post-staining, imaged, and quantified with a ChemiDoc (BioRad). The

359 percentage of crRNA spacers cleaved was calculated as a ratio of the intensity of the product band

360 relative to the total intensity of both the product and uncleaved crRNA normalized to background.

361

362 **Product size mapping and 3' end chemistry identification**

363 Cleavage product length was determined biochemically by comparing the gel migration of

364 AcrVA1-triggered cleavage products with alkaline hydrolysis and RNase T1 digestion ladders of

365 the matched untreated crRNA. Hydrolysis ladders were generated by incubating 15 nM 5'-

366 radiolabeled crRNA at 95°C for 10 min in 1X alkaline hydrolysis buffer (Ambion). Reactions were

367 quenched in 1.5X formamide loading buffer and immediately loaded to a urea-denaturing PAGE

368 (0.5X TBE) gel. For RNase T1 digestion ladders, 15 nM 5'-radiolabeled crRNA were unfolded in

369 1X RNA sequencing buffer (Ambion) at 65°C for 5 min and cooled to ambient temperature before

370 the addition of 1 U of RNase T1 (Ambion). After incubating at ambient temperature for 15 min,

371 reactions were extracted in phenol-chloroform (pH 8.0) and stored in 1.5X formamide loading

372 buffer before loading to a urea-denaturing PAGE (0.5X TBE) gel. For 3' end chemistry

373 identification, products from AcrVA1-triggered crRNA truncation reactions were extracted in

374 phenol-chloroform (pH 8.0) before incubation with 10 U of T4 polynucleotide kinase (NEB) in 1X

375 T4 polynucleotide kinase buffer (NEB) for 30 min at 37°C. Reactions were quenched with 1.5X

376 formamide loading buffer for 3 min at 95°C and resolved on a 15% (v/v) urea-denaturing PAGE

377 (0.5X TBE) gel and visualized by phosphoroimaging (Amersham Typhoon, GE Healthcare).

378

379 **RNA electrophoretic mobility-shift assays**

380 All experiments were equilibrated in 1X binding buffer (20 mM Tris-Cl (pH 7.5), 150 mM KCl, 5

381 mM MgCl2, 1mM DTT, 5% (v/v) glycerol, 50 µg mL^{-1} heparin, 50 µg mL^{-1} BSA, and 0.01% (v/v)

382 IGEPAL CA-630). Cas12a ^{32}P-crRNA EMSAs were prepared by a titration of Cas12a (0 nM, 0.063

383 nM, 0.25 nM, 1 nM, 4 nM , 16 nM, 64 nM, 256 nM) in the presence or absence of an excess of

384 AcrVA (5 µM) incubated for 30 min at 37°C before the addition of 0.2 nM ^{32}P-crRNA and

385 incubation for 30 min at 37°C.

386

387 **DNA electrophoretic mobility-shift assays**

388 All experiments were equilibrated in 1X binding buffer. To avoid the dissociation of the

389 dLbCas12a-crRNA or LbCas12a-crRNA complex during DNA binding experiments, Cas12a ^{32}P-

390 DNA EMSAs were prepared as an excess of Cas12a (960 nM) incubated with a titration of crRNA

391 (0 pM, 2.4 pM, 9.7 pM, 39 pM, 0.156 nM, 0.625 nM, 2.5 nM, 10 nM, 40 nM) to pre-form the RNP

392 for 30 min at 37°C, unless otherwise indicated. For experiments testing if AcrVA block ssDNA or

393 dsDNA binding, the RNP was first incubated with an excess of AcrVA (10 µM) for 30 min at 37°C

394 before incubation with ^{32}P-DNA substrate (0.1 nM) for 30 min at 37°C, unless indicated otherwise.

395 For experiments testing if AcrVA could disrupt a dLbCas12a-ssDNA bound complex, RNP was

396 prepared as described above except ^{32}P-ssDNA addition preceded the addition of AcrVA (10 µM),

397 cold non-target strand, and/or cold ssDNA competitor. For experiments testing if AcrVA could

398 disrupt a dLbCas12a-dsDNA or LbCas12a-crRNA bound complex, RNP was prepared at 40 nM

399   effective concentration as described above before pre-forming a DNA bound state with ^{32}P-dsDNA

400   (0.1 nM) for 30 min at 37°C. This was followed by the addition of AcrVA or cold DNA competitor

401   (0 nM, 1 nM, 3 nM, 16 nM, 80 nM, 400 nM, 2μM, 10 μM) for another 30 min at 37°C. To test

402   ATP dependence, an excess of Cas12a (960 nM) was incubated with a titration of crRNA (0 pM,

403   2.4 pM, 9.7 pM, 39 pM, 0.156 nM, 0.625 nM, 2.5 nM, 10 nM, 40 nM, 160 nM, 640 nM) to pre-

404   form the RNP for 30 min at 37°C before the addition of ^{32}P-dsDNA (0.1 nM) with or without 1

405   μM apyrase (NEB) or 2 μM ATP (NEB) and further incubation for 30 min at 37°C. AcrVA4 (10

406   uM) was then introduced for a final incubation at 37°C for 30 min. For all EMSAs, the resulting

407   complexes were resolved by 6% (v/v) native PAGE (0.5X TBE supplemented with 5 mM $MgCl_2$),

408   visualized by phosphoroimaging (Amersham Typhoon, GE Healthcare), and quantified with

409   ImageQuant (GE Healthcare). The fraction bound was determined as the ratio of the bound band

410   intensity relative to the total intensity of both the unbound and bound intensity normalized to

411   background and fit to a binding isotherm (Prism7, GraphPad) to calculate the dissociation constants

412   (*n* = 3 independent measurements). Affinities and their associated standard deviations are reported

413   in the figure legends.

414

415   **Size-exclusion chromatography and coupled di-angle light scattering**

416   All experiments were run in 20 mM HEPES.K (pH 7.5), 200 mM KCl, 1 mM TECP, 1 mM $MgCl_2$)

417   on a Superdex 10/300 Increase column (GE Healthcare) at 0.5 mL min^{-1} using the Infinity 1260

418   Bio-SEC with light scattering module (Agilent). Light scattering was collected at 15° and 90° using

419   a 658 nm laser. The system was calibrated using a 2 mg/mL BSA and dn/dc of 0.185[36]. Calibration

420   constants were determined as: 280 nm UV = 567.9, LS 90° = 39111.5 and LS 15° =29921.9. LS

421   15° data were not used in our calculations. Cas12a and AcrVA concentrations were determined via

422   nanodrop before combination with nucleic acid substrates and used as manual inputs for the mass

423   calculation and a dn/dc of 0.185. All masses were determined using a first degree fit over the linear

424   region of mass estimates for each peak using the Bio-SEC software V A.02.01 (Agilent).

425

Single particle negative stain electron microscopy

427 Purified LbCas12a RNP bound to AcrA4 was prepared at ~50 nM and negatively stained in 2%

428 (w/v) uranyl acetate (Electron Microscopy Sciences) solution following the standard deep-stain

429 procedure on holey carbon-coated EM copper grids covered with a thin layer of continuous carbon.

430 Negative stained specimens were mounted on a transmission electron microscope holder and

431 examined by a Tecnai Spirit electron microscope operated at 120-kV acceleration voltage.

432 Magnified digital micrographs of the specimen were taken at a nominal magnification of 51,000

433 on a Gatan Ultrascan4000 CCD camera with a pixel size of 2.18-Å at the specimen level by

434 Leginon[37]. The defocus values ranged from -0.9 μm to -1.5 μm, and the total accumulated dose at

435 the specimen was about 60 electrons per $Å^2$. Image analysis was performed in Appion[38].

436

REFERENCES

1. Wright, A. V., Nuñez, J. K. & Doudna, J. A. Biology and Applications of CRISPR Systems: Harnessing Nature's Toolbox for Genome Engineering. *Cell* **164,** 29–44 (2016).

2. Brouns, S. J. J. *et al.* Small CRISPR RNAs Guide Antiviral Defense in Prokaryotes. *Science (80-.).* **321,** 960–964 (2008).

3. Marraffini, L. A. & Sontheimer, E. J. CRISPR interference limits horizontal gene transfer in staphylococci by targeting DNA. *Science (80-.).* **322,** 1843–1845 (2008).

4. Barrangou, R. *et al.* CRISPR provides acquired resistance against viruses in prokaryotes. *Science (80-.).* **315,** 1709–1712 (2007).

5. Garneau, J. E. *et al.* The CRISPR/Cas bacterial immune system cleaves bacteriophage and plasmid DNA. *Nature* **468,** 67–71 (2010).

6. van Houte, S. *et al.* The diversity-generating benefits of a prokaryotic adaptive immune system. *Nature* **532,** 385–388 (2016).

7. Pawluk, A., Davidson, A. R. & Maxwell, K. L. Anti-CRISPR: Discovery, mechanism and function. *Nature Reviews Microbiology* **16,** 12–17 (2018).

8. Bondy-Denomy, J., Pawluk, A., Maxwell, K. L. & Davidson, A. R. Bacteriophage genes that inactivate the CRISPR/Cas bacterial immune system. *Nature* **493,** 429–432 (2012).

9. Bondy-Denomy, J. Protein Inhibitors of CRISPR-Cas9. *ACS Chem. Biol.* **13,** 417–423 (2018).

10. Borges, A. L. *et al.* Bacteriophage Cooperation Suppresses CRISPR-Cas3 and Cas9 Immunity. *Cell* **174,** 917–925.e10 (2018).

11. Dong, D. *et al.* Structural basis of CRISPR–SpyCas9 inhibition by an anti-CRISPR protein. *Nature* **546,** 436–439 (2017).

12. Shin, J. *et al.* Disabling Cas9 by an anti-CRISPR DNA mimic. *Sci. Adv.* **3,** e1701620 (2017).

13. Harrington, L. B. *et al.* A Broad-Spectrum Inhibitor of CRISPR-Cas9. *Cell* **170,** 1224–

463   1233.e15 (2017).

464 14. Watters, K. E., Fellmann, C., Bai, H. B., Ren, S. M. & Doudna, J. A. Systematic discovery

465   of natural CRISPR-Cas12a inhibitors. *Science (80-.).* eaau5138 (2018).

466   doi:10.1126/science.aau5138

467 15. Marino, N. D. *et al.* Discovery of widespread Type I and Type V CRISPR-Cas inhibitors.

468   *Science (80-.).* eaau5174 (2018). doi:10.1126/science.aau5174

469 16. Yamano, T. *et al.* Crystal Structure of Cpf1 in Complex with Guide RNA and Target

470   DNA. *Cell* **165,** 949–962 (2016).

471 17. Dong, D. *et al.* The crystal structure of Cpf1 in complex with CRISPR RNA. *Nature* **532,**

472   522–526 (2016).

473 18. Swarts, D. C. & Jinek, M. Cas9 versus Cas12a/Cpf1: Structure-function comparisons and

474   implications for genome editing. *Wiley Interdiscip. Rev. RNA* **9,** e1481 (2018).

475 19. Zetsche, B. *et al.* Cpf1 Is a Single RNA-Guided Endonuclease of a Class 2 CRISPR-Cas

476   System. *Cell* **163,** 759–771 (2015).

477 20. Savell, K. E. & Day, J. J. Applications of CRISPR/CAS9 in the mammalian central

478   nervous system. *Yale J. Biol. Med.* **90,** 567–581 (2017).

479 21. Sternberg, S. H., Redding, S., Jinek, M., Greene, E. C. & Doudna, J. A. DNA interrogation

480   by the CRISPR RNA-guided endonuclease Cas9. *Nature* **507,** 62–67 (2014).

481 22. Chen, J. S. *et al.* CRISPR-Cas12a target binding unleashes indiscriminate single-stranded

482   DNase activity. *Science (80-.).* **360,** 436–439 (2018).

483 23. Strohkendl, I., Saifuddin, F. A., Rybarski, J. R., Finkelstein, I. J. & Russell, R. Kinetic

484   Basis for DNA Target Specificity of CRISPR-Cas12a. *Mol. Cell* **71,** 816–824.e3 (2018).

485 24. Swarts, D. C. & Jinek, M. Mechanistic Insights into the cis- and trans-Acting DNase

486   Activities of Cas12a. *Mol. Cell* (2019). doi:10.1016/j.molcel.2018.11.021

487 25. Knott, G. J. & Doudna, J. A. CRISPR-Cas guides the future of genetic engineering.

488   *Science (80-.).* **361,** 866–869 (2018).

489   26.   Bondy-Denomy, J. Protein Inhibitors of CRISPR-Cas9. *ACS Chem. Biol.* **13,** 417–423

490   (2018).

491   27.   Swarts, D. C., van der Oost, J. & Jinek, M. Structural Basis for Guide RNA Processing and

492   Seed-Dependent DNA Targeting by CRISPR-Cas12a. *Mol. Cell* **66,** 221–233.e4 (2017).

493   28.   Landsberger, M. *et al.* Anti-CRISPR Phages Cooperate to Overcome CRISPR-Cas

494   Immunity. *Cell* **174,** 908–916.e12 (2018).

495   29.   Stella, S. *et al.* Conformational Activation Promotes CRISPR-Cas12a Catalysis and

496   Resetting of the Endonuclease Activity. *Cell* **175,** 1856–1871.e21 (2018).

497   30.   Burstein, D. *et al.* New CRISPR-Cas systems from uncultivated microbes. *Nature* **542,**

498   237–241 (2017).

499   31.   Shmakov, S. *et al.* Discovery and Functional Characterization of Diverse Class 2 CRISPR-

500   Cas Systems. *Mol. Cell* **60,** 385–397 (2015).

501   32.   Katoh, K. & Standley, D. M. MAFFT Multiple Sequence Alignment Software Version 7:

502   Improvements in Performance and Usability. *Mol. Biol. Evol.* **30,** 772–780 (2013).

503   33.   Stamatakis, A. RAxML version 8: a tool for phylogenetic analysis and post-analysis of

504   large phylogenies. *Bioinformatics* **30,** 1312–1313 (2014).

505   34.   Letunic, I. & Bork, P. Interactive tree of life (iTOL) v3: an online tool for the display and

506   annotation of phylogenetic and other trees. *Nucleic Acids Res.* **44,** W242–W245 (2016).

507   35.   East-Seletsky, A. *et al.* Two distinct RNase activities of CRISPR-C2c2 enable guide-RNA

508   processing and RNA detection. *Nature* **538,** 270–273 (2016).

509   36.   Zhao, H., Brown, P. H. & Schuck, P. On the Distribution of Protein Refractive Index

510   Increments. *Biophys. J.* **100,** 2309–2317 (2011).

511   37.   Suloway, C. *et al.* Automated molecular microscopy: The new Leginon system. *J. Struct.*

512   *Biol.* **151,** 41–60 (2005).

513   38.   Lander, G. C. *et al.* Appion: An integrated, database-driven pipeline to facilitate EM image

514   processing. *J. Struct. Biol.* **166,** 95–102 (2009).

515 **ACKNOWLEDGMENTS**

525

526 **AUTHOR CONTRIBUTIONS**

527 G.J.K. conceived the study with input from K.E.W. G.J.K designed experiments with input from

528 B.W.T and J.A.D. G.J.K and B.W.T carried out biochemical work. M.J.L and G.J.K carried out

529 light scattering experiments. J.L carried out negative stain electron microscopy. B.A.S carried out

530 bioinformatic analysis. G.J.K drafted the manuscript and all authors edited the manuscript.

531

532 **AUTHOR INFORMATION**

537

538 **COMPETING INTERESTS**

539 The Regents of the University of California have patents pending for CRISPR technologies on

540 which the authors are inventors.

541   **Extended Data Table 1 | Oligonucleotides used in this study**

Oligo ID	Name*	Sequence⬥	Main Text Figures	Extended Data Figures
rGJK_004	MbCas12a pre-crRNA (24-nt T1)	GACCUUUUAAAUUUCUACUGUUUGUAGAU**AAAGUGCUCAUCAUUGGAAAACGU**	-	8a
rGJK_005	MbCas12a crRNA (24-nt T1)	AAUUUCUACUGUUUGUAGAU**AAAGUGCUCAUCAUUGGAAAACGU**	4a, 5a	8b-c, 9d
rGJK_006	LbCas12a pre-crRNA (24-nt T1)	AGAUUAAAUAAUUUCUACUAAGUGUAGAU**AAAGUGCUCAUCAUUGGAAAACGU**	-	8a, 10c
rGJK_007	LbCas12a crRNA (24-nt T1)	AAUUUCUACUAAGUGUAGAU**AAAGUGCUCAUCAUUGGAAAACGU**	4a-d, 5a-c `	8b-c, 9a, 9d-g, 10b
rGJK_008	AsCas12a pre-crRNA (24-nt T1)	GACCUUUUUAAUUUCUACUCUUGUAGAU**AAAGUGCUCAUCAUUGGAAAACGU**	-	8a
rGJK_009	AsCas12a crRNA (24-nt T1)	AAUUUCUACUCUUGUAGAU**AAAGUGCUCAUCAUUGGAAAACGU**	4a, 5a	8b-c, 9d
rGJK_011	LbCas12a crRNA (20-nt T1)	AAUUUCUACUAAGUGUAGAU**AAAGUGCUCAUCAUUGGAAA**	-	9b
rGJK_014	LbCas12a crRNA (24-nt T2)	AAUUUCUACUAAGUGUAGAU**GCUCCAGAUUUAUCAGCAAUAAAC**	2b, 2c	5b-d, 9a
rGJK_016	MbCas12a crRNA (20-nt T3)	AAUUUCUACUGUUUGUAGAU**GAUCGUUACGCUAACUAUGA**	1c	3a
rGJK_017	LbCas12a crRNA (20-nt T3)	AAUUUCUACUAAGUGUAGAU**GAUCGUUACGCUAACUAUGA**	1b-d, 2a, 2d, 2e, 3a-b	1a-d, 3b, 4a-b, 6a-c, 7a-d
rGJK_018	AsCas12a crRNA (20-nt T3)	AAUUUCUACUCUUGUAGAU**GAUCGUUACGCUAACUAUGA**	1c	3c
rGJK_021	LbCas12a crRNA (18-nt T1)	AAUUUCUACUAAGUGUAGAU**AAAGUGCUCAUCAUUGGA**	-	9b
rGJK_022	LbCas12a crRNA (12-nt T1)	AAUUUCUACUAAGUGUAGAU**AAAGUGCUCAUC**	-	9b
rGJK_023	LbCas12a crRNA (6-nt T1)	AAUUUCUACUAAGUGUAGAU**AAAGUG**	-	9b
rGJK_035	LbCas12a crRNA (4-nt T3)	AAUUUCUACUAAGUGUAGAU**GAUC**	-	10a
rGJK_036	crRNA spacer (16-nt T3)	**GUUACGCUAACUAUGA**	-	10a
dGJK_001	NT-DNA strand (24-nt T1)	GTGGCCGTTTA**AAAGTGCTCATCATTGGAAAACGT**AGGATGGGCACCAC	-	8c
dGJK_002	T-DNA strand (24-nt T1)	GTGGTGCCCATCCT**ACGTTTTCCAATGATGAGCACTTT**TAAACGGCCAC	-	8c
dGJK_006	NT-DNA strand (T3)	GACGACAAAACTTTA**GATCGTTACGCTAACTATGA**GGGCTGTCTGTGGAATGCTA	1b-c, 2a, 2d-e, 3a-b	1a-d, 5a, 6a-c, 7a, 7d
dGJK_007	T-DNA strand (T3)	TAGCATTCCACAGACAGCCC**TCATAGTTAGCGTAACGATC**TAAAGTTTTGTCGTC	1b-d, 2a, 2d-e, 3a-b	1a-d, 3a-c, 4a-b, 5a, 6a-c, 7a-d
dGJK_010	NT-DNA strand (T3) Mismatched all	GACGACAAAACTTTA**CTAGCAATGCGATTGATACT**GGGCTGTCTGTGGAATGCTA	-	7a-b
dGJK_012	NT-DNA strand (T3) Mismatched 5'	GACGACAAAACTTTA**CTAGCTTACGCTAACTATGA**GGGCTGTCTGTGGAATGCT A	-	7c
dGJK_013	NT-DNA strand (T3) Mismatches 3'	GACGACAAAACTTTA**GATCGTTACGCTAACATACT**GGGCTGTCTGTGGAATGCTA	-	7c
dGJK_014	NT-DNA strand (T3) Mismatches middle	GACGACAAAACTTTA**GATCGTTAGCGATACTATGA**GGGCTGTCTGTGGAATGCTA	-	7c
rGJK_453	*trans*-ssRNA substrate	AUGGCAGCGCCUCUUGCAACGAUUAAAUACUGCUUCUAUAUACGGCAUACACCGUUUCGG	-	9c

542   * Abbreviations: T1–Ampicillin resistance gene target; T2– Ampicillin resistance gene target; T3 – Target sequence used in[22].   ⬥ Spacer or targets sequences are shown in bold.
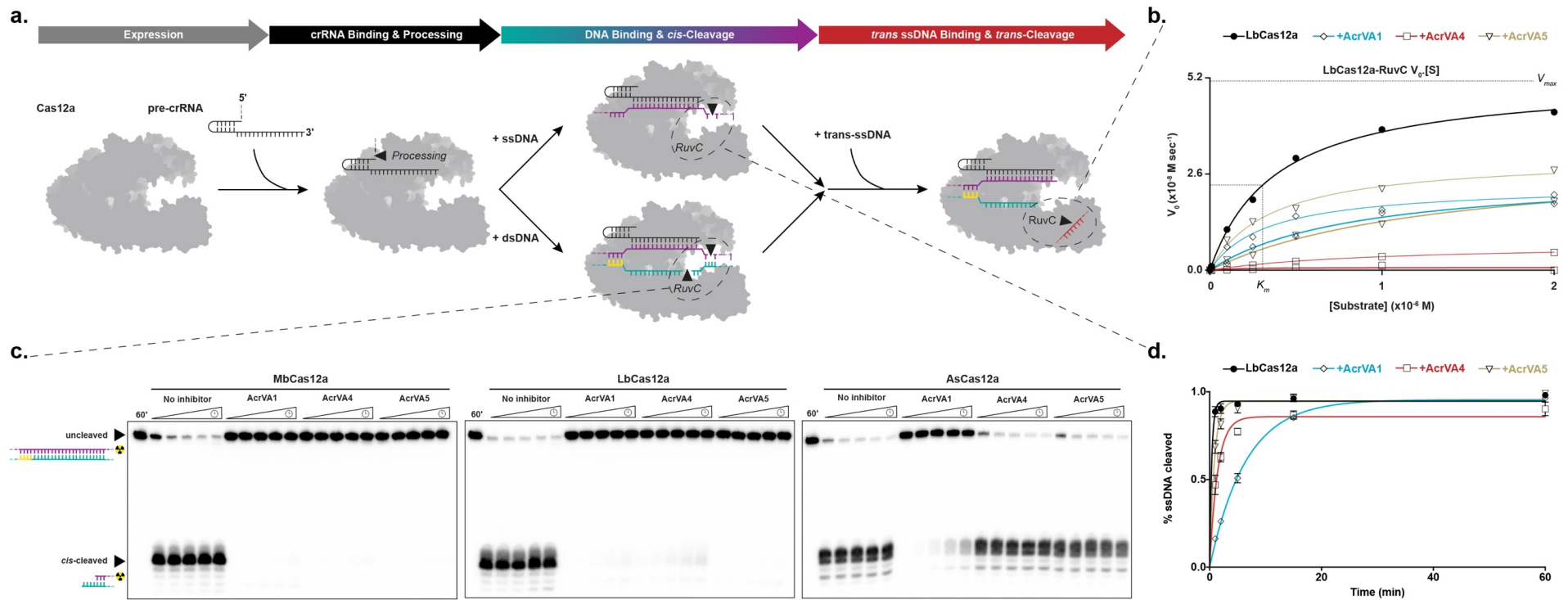
543 **Figure 1 – AcrVAs do not inhibit all modes of DNA targeting by Cas12a. a)** Schematic representation of the steps in Cas12a target interference,

544 **b)** Michaelis-Menten fit for 0.1 nM effective LbCas12a holoenzyme in the absence (black) or presence of AcrVA1, AcrVA4, or AcrVA5. The mean

545 initial velocity (V_0) is plotted against increasing DNase-Alert substrate concentrations (µM), where $n = 3$ replicates. The *Vmax* and *K*m for wild-type

546 LbCas12a RuvC are indicated with dashed lines. **c)** Radiolabeled kinetic dsDNA cleavage assays for (left to right) MbCas12a, LbCas12a, and

547 AsCas12a complexes with or without AcrVAs. Time courses represent 1', 2', 5', 15', and 60'. The uncleaved and *cis*-cleaved fractions are indicated

548 with black triangles, **d)** Quantified percentage ssDNA cleaved for LbCas12a in the presence or absence of AcrVAs (mean ± sd, $n = 3$). Experimental

549 fits are shown as solid lines and the calculated pseudo-first-order rate constants (k_{obs}) (mean ± sd) are 2.6 ± 0.3 min^{-1}, 0.15 ± 0.01 min^{-1}, 0.7 ± 0.06

550 min^{-1}, and 1.2 ± 0.09 min^{-1} for LbCas12a, LbCas12a+AcrVA1, LbCas12a+AcrVA4, and LbCas12a+AcrVA5 respectively.

a.

b.

c.
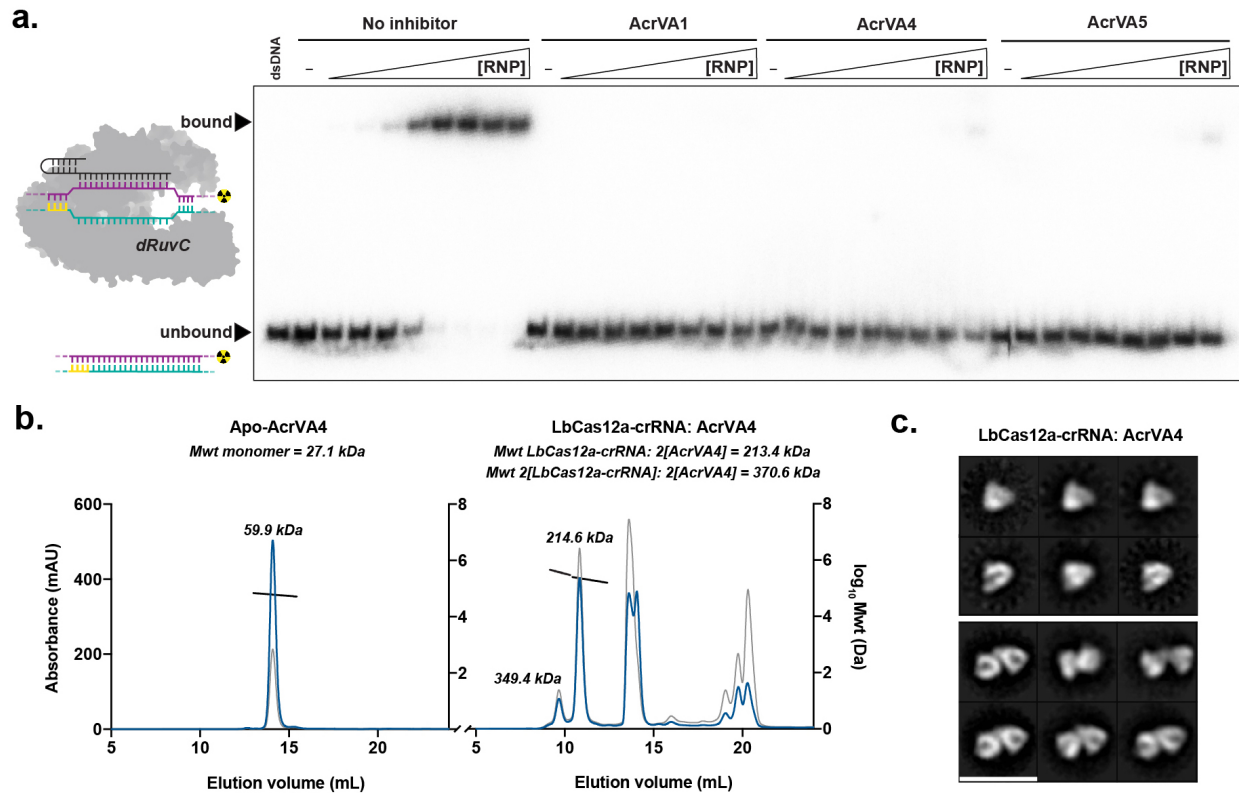
Figure 2 – AcrVAs block dsDNA binding and AcrVA4 dimerizes Cas12a. a) Radiolabeled dsDNA electrophoretic mobility shift assay of increasing concentrations of dLbCas12a-crRNA complexed with or without AcrVA before association with dsDNA. The bound and unbound fractions are indicated with black triangles, **b)** Size exclusion chromatography coupled light scattering traces for (left) AcrVA4 alone and (right) LbCas12a-crRNA complexed with AcrVA4. The absorbance at 280 nm (blue) and 260 nm (grey) are shown (left axis) with the linear region for the mass estimate corresponding to the relevant peaks (black lines, central and right axis). The predicted molecular weights for each sample are shown above the graph and the calculated molecular weights are indicated adjacent to the relevant peak **c)** 2D-class averages of LbCas12a-crRNA monomers (top) and LbCas12a-crRNA dimers bound to AcrVA4 (bottom). The scale bar represents 28 nm.

a.

b.
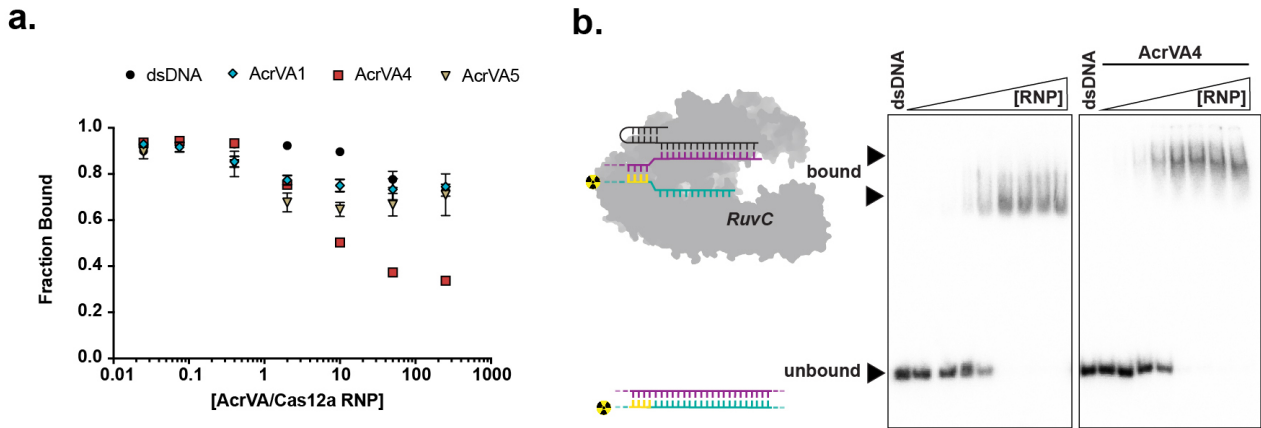
574 **Figure 3 – AcrVA4 displaces dsDNA bound to dCas12a but not wild-type Cas12a**. **a)**
575 Quantified fraction dsDNA bound by dLbCas12a-crRNA after complexing with dsDNA before the
576 addition of increasing concentrations of AcrVA or dsDNA competitor determined by EMSA (mean
577 ± sd, *n* = 3), **b)** Radiolabeled dsDNA electrophoretic mobility shift assay of increasing
578 concentrations of LbCas12a-crRNA first complexed with dsDNA before addition of AcrVA. The
579 bound and unbound fractions are indicated with black triangles.
580
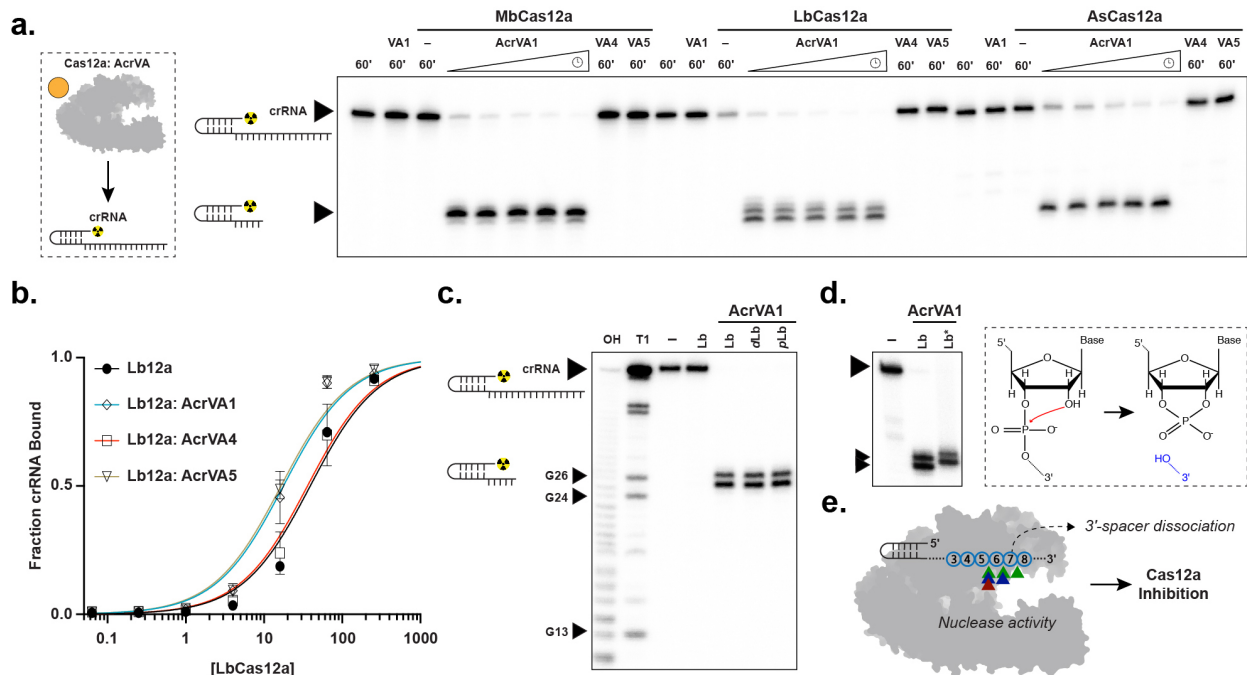
Figure 4 – AcrVA1-triggered endoribonuclease activity truncates a Cas12a-bound crRNA. a) Radiolabeled kinetic crRNA cleavage assays for (left to right) MbCas12a, LbCas12a, and AsCas12a complexed with or without AcrVAs. Time courses represent 1, 2, 5, 15, and 60 min. Black triangles indicate full-length and truncated crRNA, **b)** Quantified fraction crRNA bound by LbCas12a in the presence or absence of AcrVAs determined by EMSA (mean ± sd, *n* = 3). Measured dissociation constants (Kd) are 38.9 nM ± 4.7, 17.6 ± 2.4, 35.8 ± 4.4, and 16.4 ± 2.1 in absence of inhibitor or in the presence of AcrVA1, AcrVA4, or AcrVA5, respectively, **c)** Radiolabeled crRNA cleavage assay with LbCas12a-crRNA complexed without or with AcrVA1. Treatments in the absence of AcrVA1 are (left to right) crRNA hydrolysis ladder (OH), crRNA RNase T1 digestion (T1), untreated crRNA (-), and crRNA incubated with LbCas12a (Lb). Treatments in the presence of AcrVA1 are (left to right) wild-type LbCas12a (Lb), dLbCas12a (D832A, dLb), and processing dead Cas12a (K785A, pLb). A large black triangle indicates the full-length crRNA, smaller triangles indicate RNase T1 mapped G-nucleotides, **d)** Radiolabeled crRNA cleavage assay using LbCas12a-crRNA complexed with AcrVA1 that is either untreated (Lb) or treated with PNK (Lb*), **e)** Schematic representation of AcrVA1-triggered crRNA spacer cleavage activity on Cas12a. Cleavage sites for Mb (blue), Lb (green), and AsCas12a (red) are indicated with triangles.
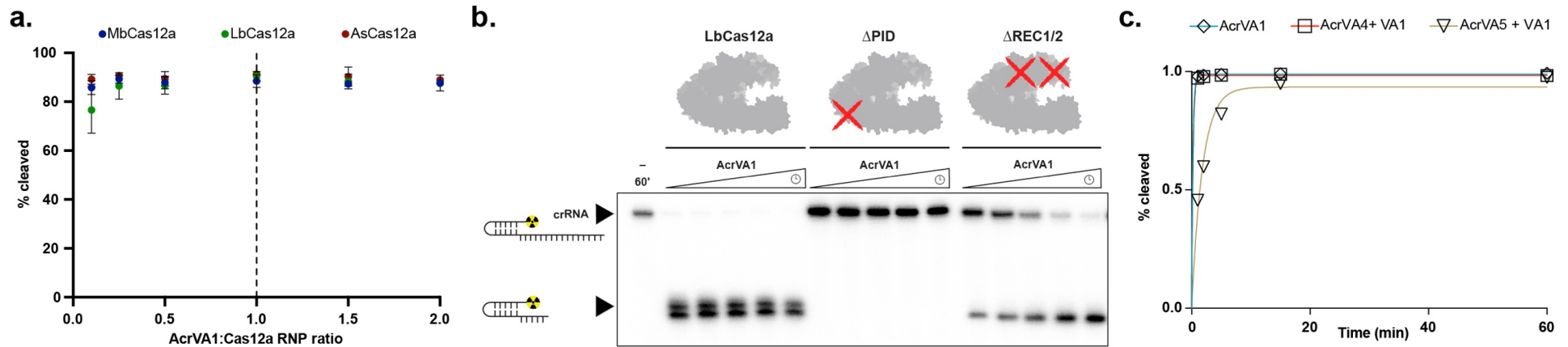
Figure 5 – AcrVA1-triggered endoribonuclease activity is multiple turnover, requires the PID, and competes with AcrVA5. a) Percentage crRNA spacers truncated after 1 hr at different ratios of AcrVA1:Cas12a-crRNA (mean ± sd, $n = 3$). **b)** Radiolabeled kinetic crRNA cleavage assays for (left to right) LbCas12a, ΔPID LbCas12a, and ΔREC1/2 LbCas12a in the presence of AcrVA1. Time courses represent 1, 2, 5, 15, and 60 min. Black triangles indicate the full-length and truncated crRNA. The approximate position of the truncated domains is shown with a red cross. **c)** Quantified time-course of percentage AcrVA1-triggered spacers truncated in the presence AcrVA4 or AcrVA5 ($n = 3$). Experimental fits are shown as solid lines and the calculated pseudo-first-order rate constants (k_{obs}) (mean ± sd) are $4.8 ± 0.2$ min^{-1}, $4.4 ± 0.3$ min^{-1}, and $0.5 ± 0.04$ min^{-1} for AcrVA1, AcrVA1 + AcrVA4, and AcrVA1 + AcrVA5, respectively.
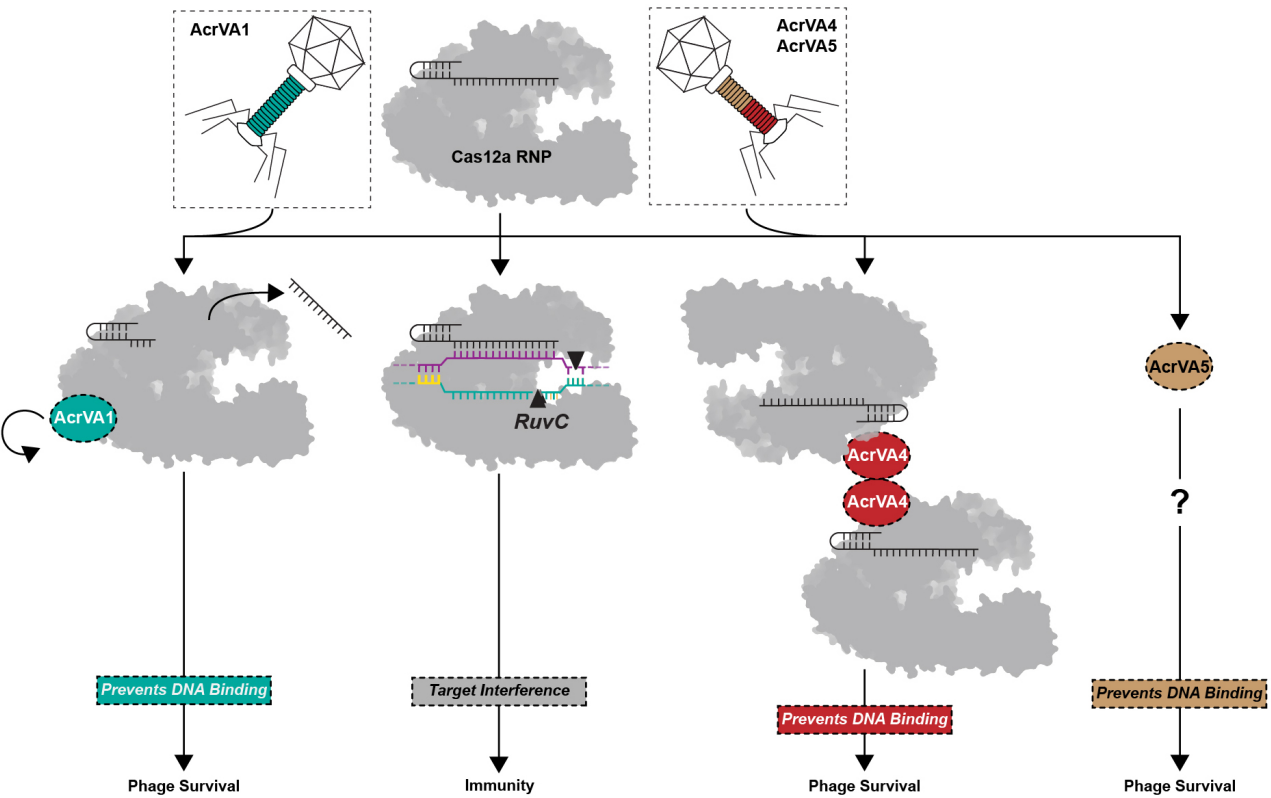
606
607 **Figure 6 – Three distinct modes of CRISPR-Cas12a inactivation.** Model for AcrVA1, AcrVA4,
608 and AcrVA5 inhibition of Cas12a. Cas12a assembles with its crRNA to form a surveillance
609 complex (top). In the absence of inhibitors, Cas12a recognizes a complementary target DNA
610 activating the RuvC leading to target interference and immunity. Phage-encoded AcrVA1 (teal)
611 associates with Cas12a triggering crRNA spacer truncation preventing DNA binding. Phage-
612 encoded AcrVA4 dimerizes (red) Cas12a and blocks dsDNA binding. Phage-encoded AcrVA5
613 (brown) blocks Cas12a dsDNA binding via an unknown mechanism.

1

2

3 **EXTENDED DATA**

4 **Broad-spectrum enzymatic inhibition of CRISPR-Cas12a**

5

6

7 Gavin J. Knott[1], Brittney W. Thornton[1], Marco J. Lobba[2], Junjie Liu[1], Basem Al-Shayeb[3], Kyle E.

8 Watters[1], and Jennifer A. Doudna[1,2,4-7*]

9

10 [1]Department of Molecular and Cell Biology, University of California, Berkeley, California, 94720,

11 USA.

12 [2]Department of Chemistry, University of California, Berkeley, California, 94720, USA.

13 [3]Department of Plant and Microbial Biology, University of California, Berkeley, CA, 94720, USA

14 [4]Molecular Biophysics & Integrated Bioimaging Division, Lawrence Berkeley National

15 Laboratory, Berkeley, USA.

16 [5]Gladstone Institutes, San Francisco, California, 94158, USA.

17 [6]Howard Hughes Medical Institute, University of California, Berkeley, California 94720, USA.

18 [7]Innovative Genomics Institute, University of California, Berkeley, California 94720, USA.

19 *Correspondence should be addressed to J.A.D (doudna@berkeley.edu).

20

21

a.

	Vmax	Km (M⁻¹) x10⁻⁸
LbCas12a (Wild-type)	5.165 ± 0.14	0.381 ± 0.03

b.

c.

d.

	$Vmax$	Km (M^{-1}) $x10^{-8}$
LbCas12a:AcrVA1 (25 nM)	2.308 ± 0.12	0.329 ± 0.05
LbCas12a:AcrVA1 (50 nM)	2.627 ± 0.22	0.833 ± 0.15

	$Vmax$	Km (M^{-1}) $x10^{-8}$
LbCas12a:AcrVA4 (25 nM)	0.715 ± 0.04	0.952 ± 0.13
LbCas12a:AcrVA4 (50 nM)	0.075 ± 0.04	0.135 ± 0.35

	$Vmax$	Km (M^{-1}) $x10^{-8}$
LbCas12a:AcrVA5 (25 nM)	3.058 ± 0.35	0.355 ± 0.05
LbCas12a:AcrVA5 (50 nM)	3.077 ± 0.15	1.317 ± 0.29

22
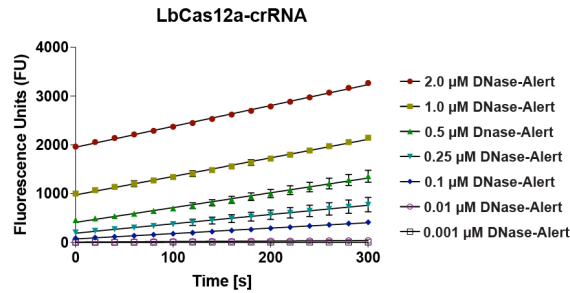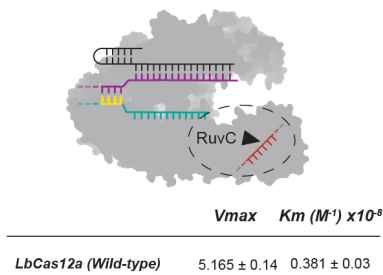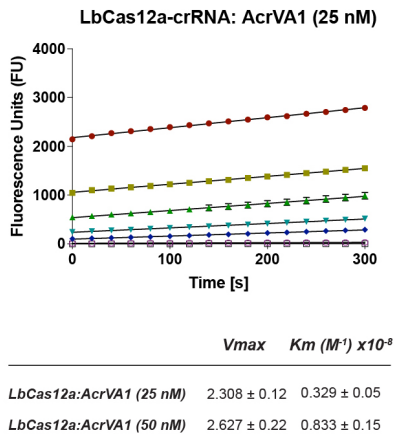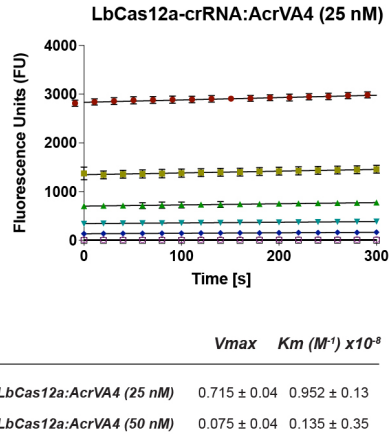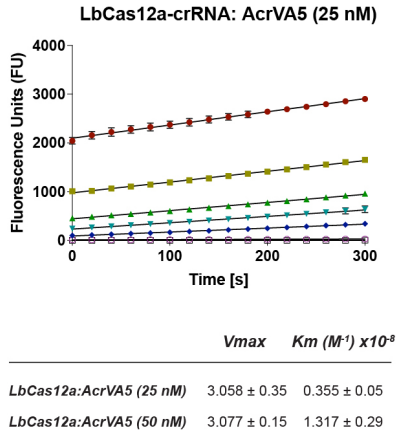
23 **Extended Data Fig. 1 – Michaelis-Menten kinetics for the LbCas12a RuvC-nuclease in the**
24 **absence or presence of AcrVAs.** Representative plots of initial velocity versus time for **a)**
25 LbCas12a-crRNA, **b)** LbCas12a-crRNA with 25 nM AcrVA1**, c)** LbCas12a-crRNA with 25 nM
26 AcrVA4, **d)** LbCas12a-crRNA with 25 nM AcrVA5. The mean calculated *Vmax* and *K*m are
27 reported in a table below (mean ± sd, *n*=3).

28

a.

b.

29
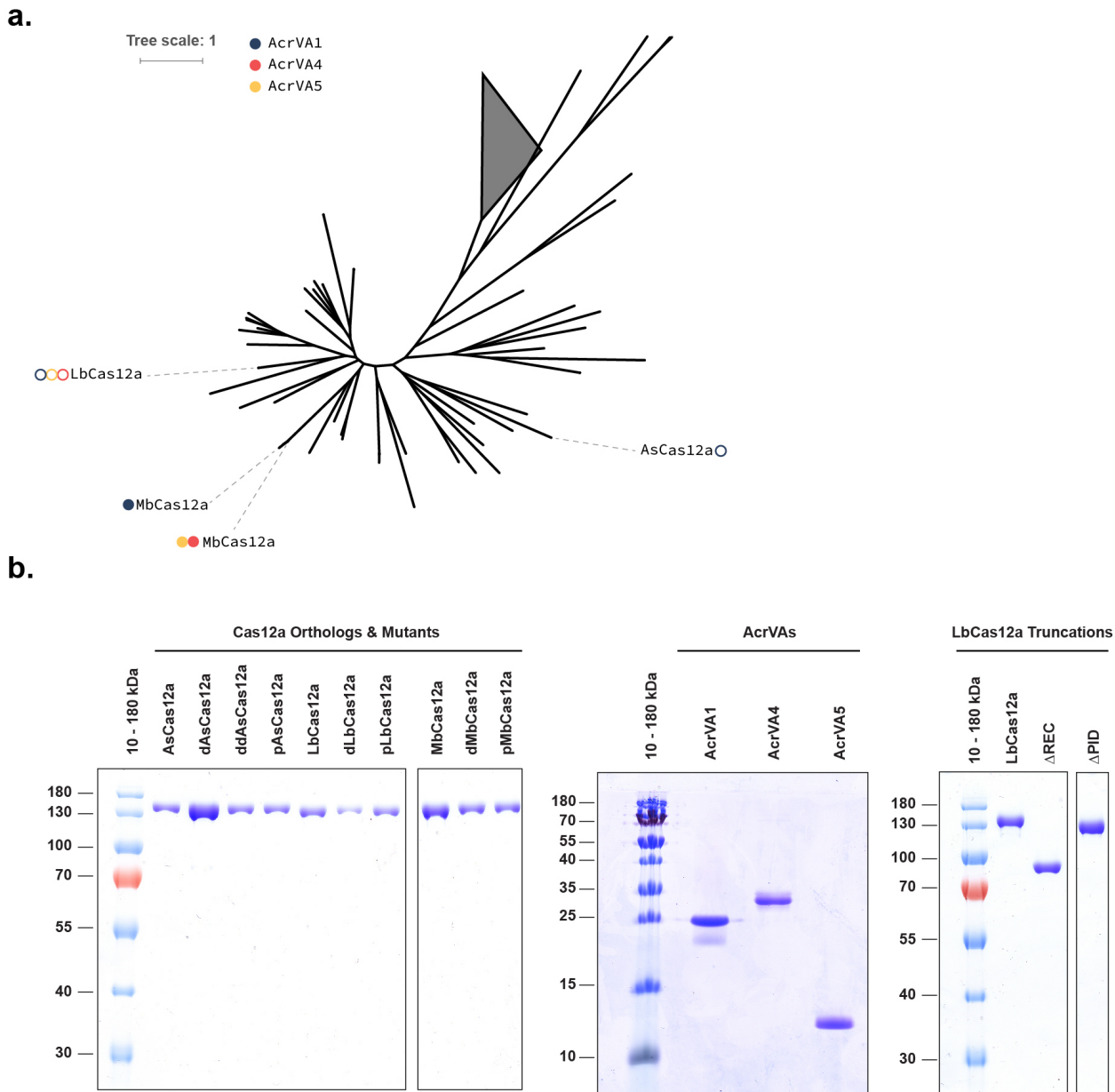
Extended Data Fig. 2 – Purified Cas12a orthologs and AcrVA used in this study. a) Unrooted Maximum Likelihood phylogenetic tree of type V effector proteins. Triangle denotes collapsed branches of Cas12b-e. Cas12a orthologs targeted by AcrVA are indicated with circles (closed circles, Cas12a orthologs that are co-occurring with the denoted prophage AcrVA proteins on the same genome; open circles, Cas12a orthologs experimentally inhibited by an AcrVA but without naturally occurring AcrVA orthologs, **b)** SDS polyacrylamide gel electrophoresis of purified proteins used in this study.
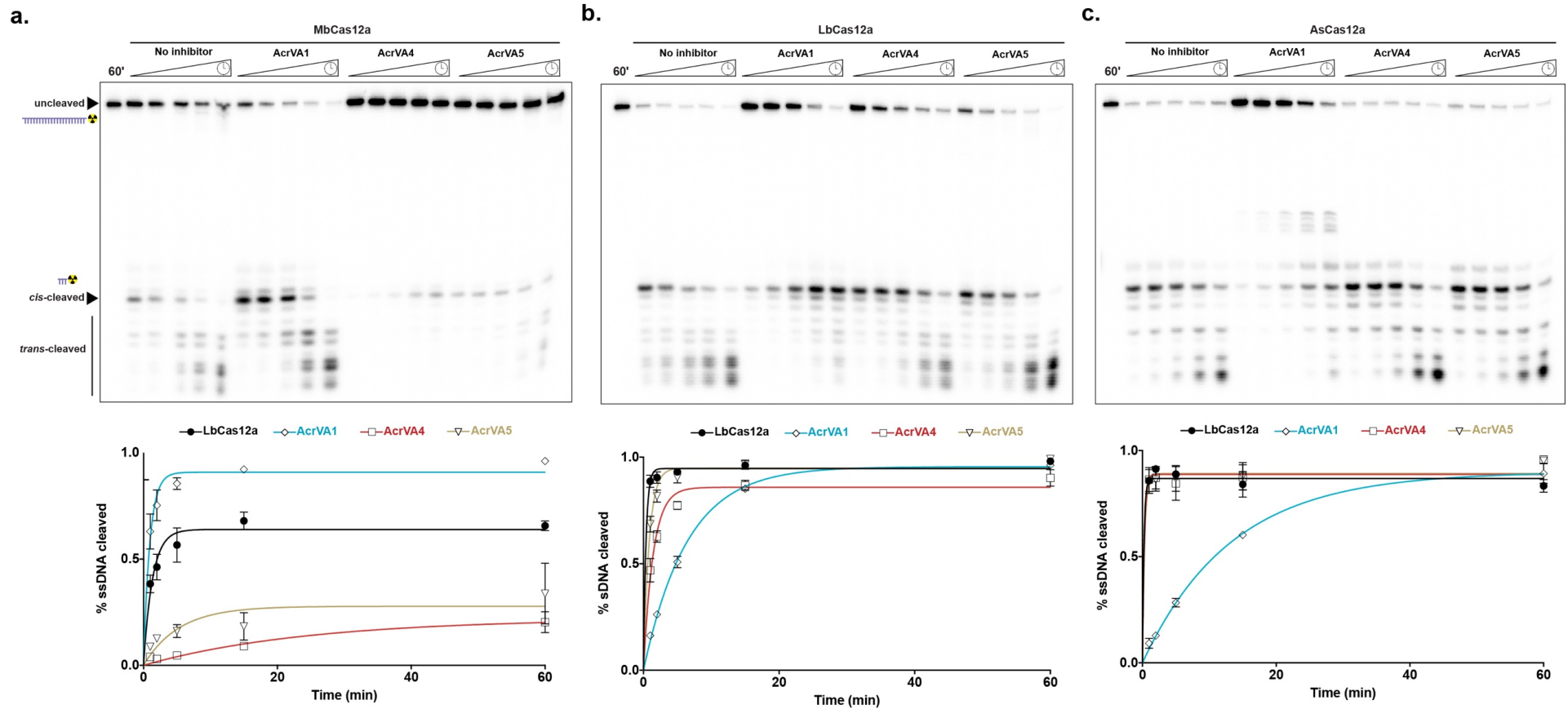
Extended Data Fig. 3 – AcrVAs differentially effect single-stranded DNA cleavage by Cas12a orthologs. (Top) Representative 5'-radiolabeled kinetic ssDNA cleavage assays for **a)** MbCas12a, **b)** LbCas12a, and **c)** AsCas12a in the absence or presence of AcrVAs. Time courses represent 1, 2, 5, 15, and 60 min. The uncleaved and *cis*-cleaved fractions are indicated with black triangles and the trans-cleavage products are indicated by a black bar. (Bottom) Quantified percentage ssDNA cleaved for **a)** MbCas12a, **b)** LbCas12a, and **c)** AsCas12a in the presence or absence of AcrVAs (mean ± sd, *n* = 3). Experimental fits are shown as solid lines and the calculated pseudo-first-order rate constants (k_{obs}) (mean ± sd, *n*=3) are: **a)** 0.7 ± 0.1 min^{-1}, 1.1 ± 0.1 min^{-1}, 0.04 ± 0.01 min^{-1}, and 0.2 ± 0.08 min^{-1} for MbCas12a, MbCas12a+AcrVA1, MbCas12a+AcrVA4, and MbCas12a+AcrVA5 respectively, **b)** 2.6 ± 0.3 min^{-1}, 0.15 ± 0.01 min^{-1}, 0.7 ± 0.06 min^{-1}, and 1.2 ± 0.09 min^{-1} for LbCas12a, LbCas12a+AcrVA1, LbCas12a+AcrVA4, and LbCas12a+AcrVA5 respectively, **c)** 4.5 ± 2.8 min^{-1}, 0.08 ± 0.01 min^{-1}, 3.5 ± 1.6 min^{-1}, and 3.1 ± 0.9 min^{-1} for AsCas12a, AsCas12a+AcrVA1, AsCas12a+AcrVA4, and AsCas12a+AcrVA5 respectively.

47
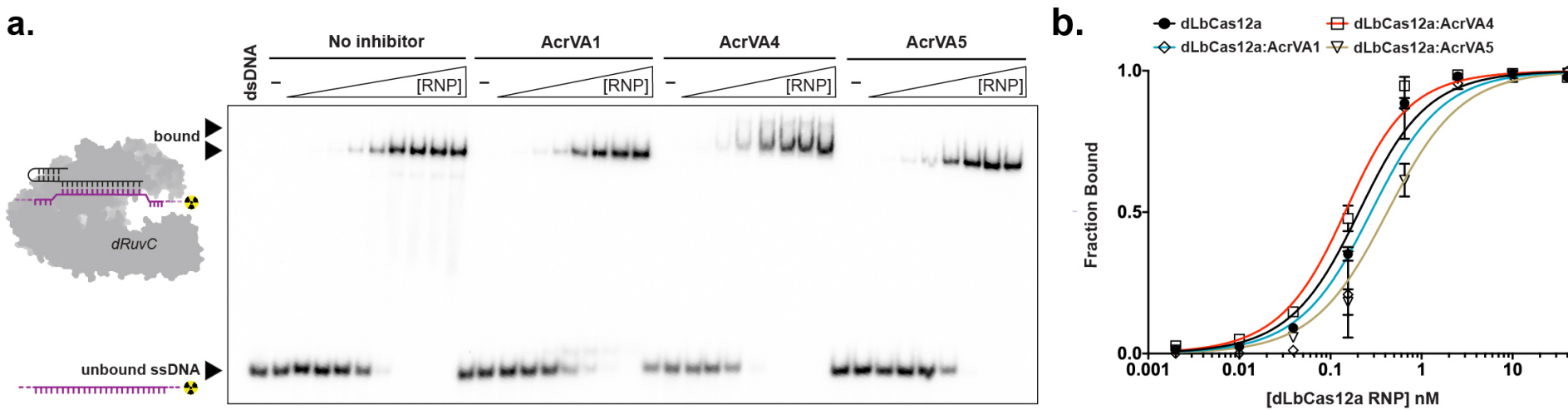
Extended Data Fig. 4 – AcrVAs do not block ssDNA binding by dLbCas12a-crRNA. a) Representative 5'-radiolabeled ssDNA EMSA to test if AcrVAs block ssDNA binding with increasing concentrations of dLbCas12a-crRNA complexed with or without AcrVA before association with ssDNA. The bound and unbound fractions are indicated with black triangles, **b)** Quantified fraction ssDNA bound by dLbCas12a in the presence or absence of AcrVAs determined by EMSA (Extended Data Fig. 4a) (mean ± sd, *n* = 3). Measured dissociation constants (Kd) are 155 pM ± 20, 229 pM ± 53, 94 pM ± 11, and 371 pM ± 45 in the absence of inhibitor or in the presence of AcrVA1, AcrVA4, or AcrVA5, respectively.
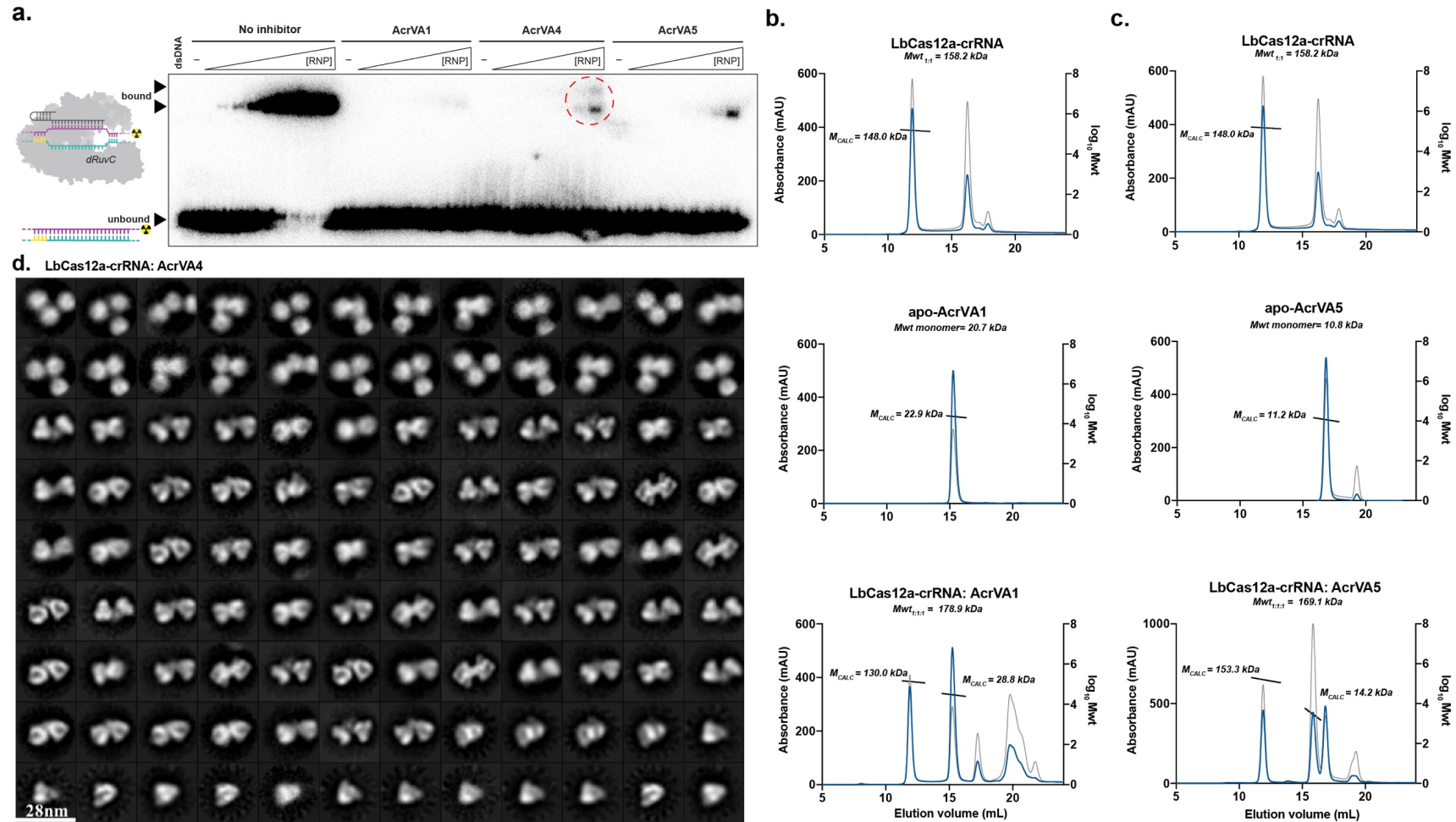
Extended Data Fig. 5 – Oligomeric state of AcrVA1, AcrVA4 and AcrVA5. a) Figure 2a shown with an adjusted exposure to highlight the presence of a super-shift (red circle). Size exclusion chromatography coupled light scattering traces for **b)** (top to bottom) LbCas12a-crRNA, apo-AcrvA1, and the LbCas12a-crRNA:AcrVA1 complex, and **c)** (top to bottom) LbCas12a-crRNA, apo-AcrvA5, and the LbCas12a-crRNA:AcrVA5 complex. The absorbance at 280 nm (blue) and 260 nm (grey) are shown (left axis) with the linear region for the mass estimate corresponding to the relevant peaks (black lines, right axis). The predicted molecular weights for each sample are shown above the graph and the calculated molecular weights are indicated adjacent to the relevant peak, **d)** 2D-class averages of LbCas12a-crRNA bound to AcrVA4. The scale bar represents 28 nm.
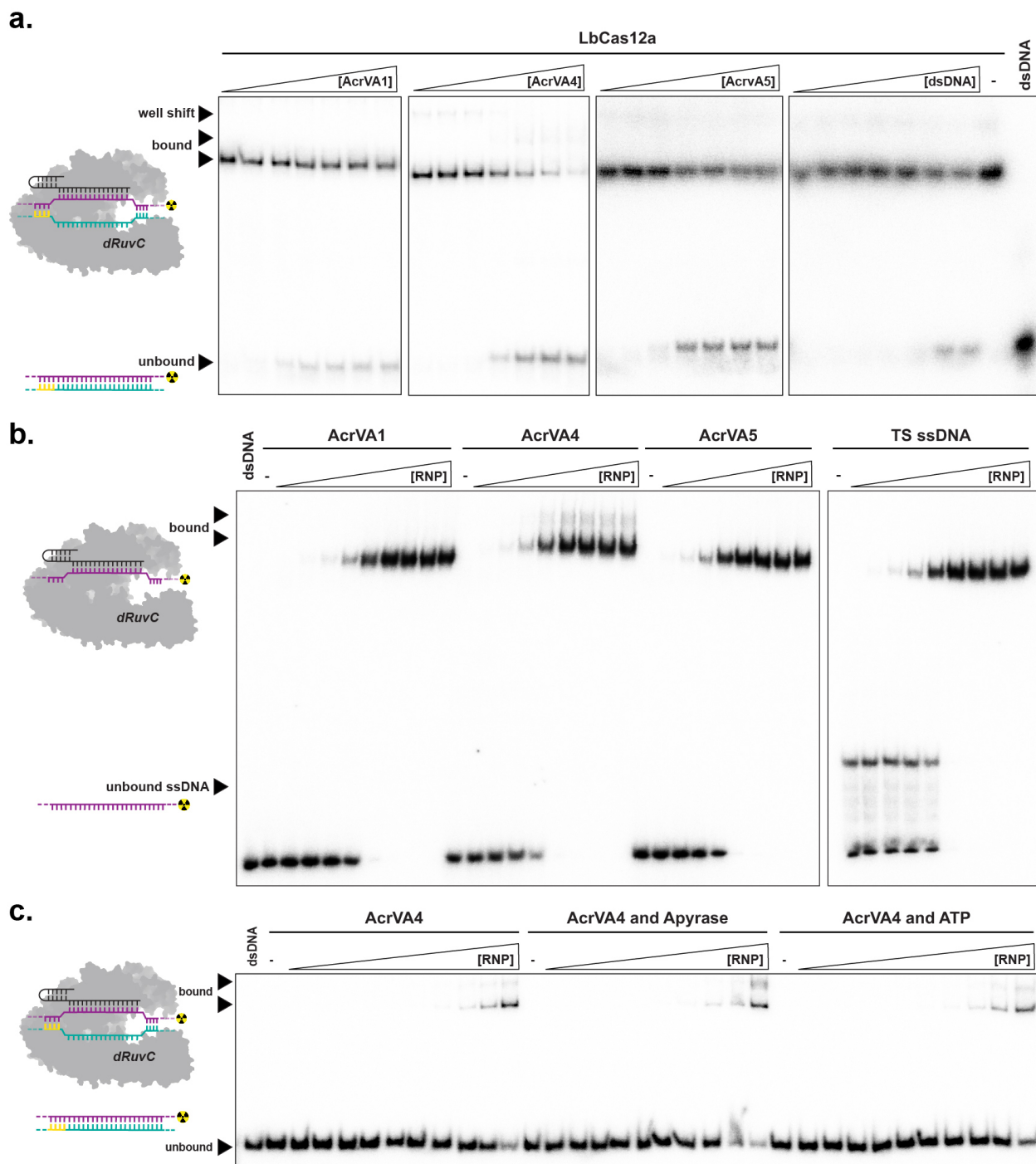
Extended Data Fig. 6 – AcrVA4 can displace dsDNA bound to dLbCas12a but not ssDNA in an ATP-independent manner. a) Representative 5'-radiolabeled dsDNA EMSAs for the quantifications presented in Figure 3a. A 40 nM effective concentration of dLbCas12a-crRNA RNP was complexed with dsDNA and then titrated against increasing concentrations of AcrVA1, AcrVA4, AcrVA5, or cold dsDNA competitor (left to right), **b)** 5'-radiolabeled ssDNA EMSA with increasing concentrations of dLbCas12a-crRNA complexed with radiolabeled ssDNA before the addition of (left to right) AcrVA1, AcrVA4, AcrVA5, or cold ssDNA competitor. **c)** 5'-radiolabeled dsDNA EMSA with increasing concentrations of dLbCas12a-crRNA complexed with dsDNA in the absence or presence of apyrase or ATP before the addition of AcrVA4. For all panels the bound and unbound fractions are indicated with black triangles.
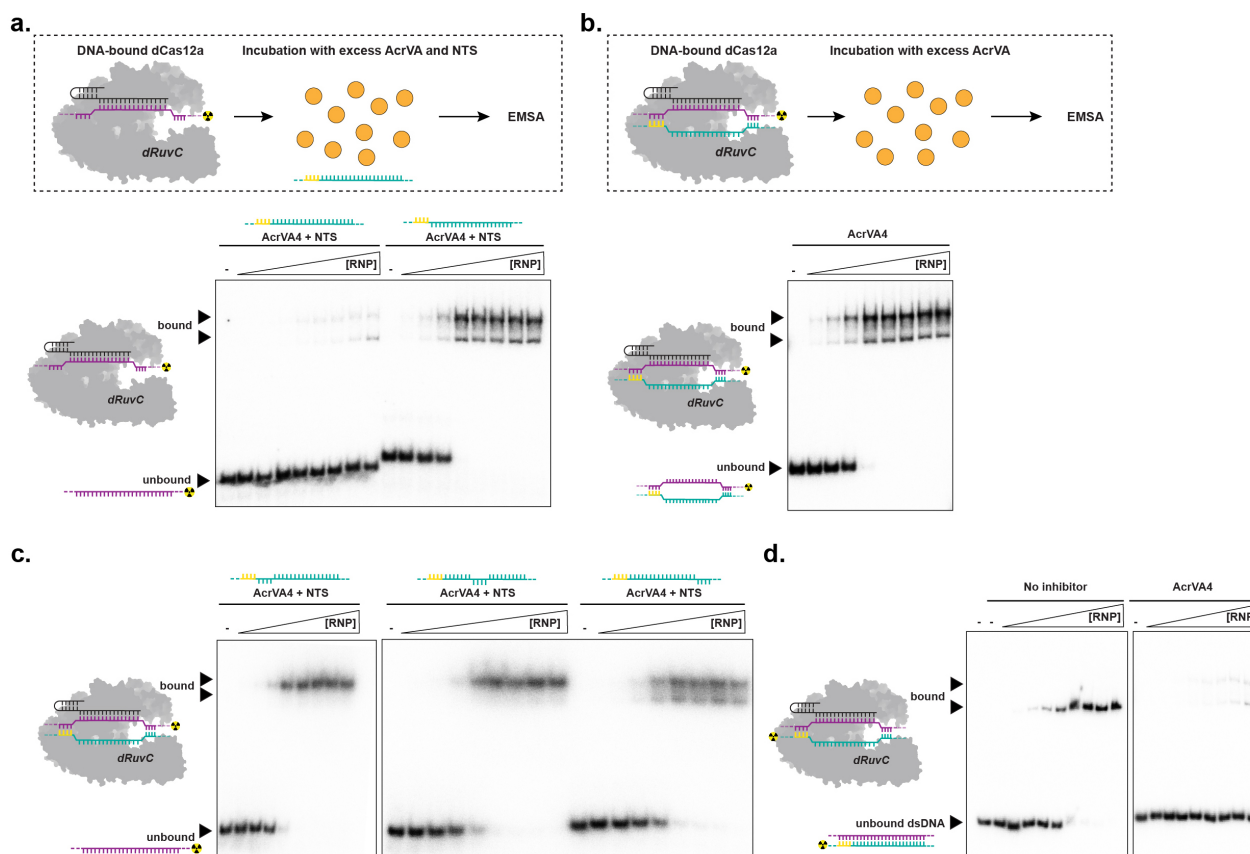
Extended Data Fig. 7 – AcrVA4 drives TS ssDNA release from dLbCas12a-crRNA in the presence of a complementary non-target strands (NTS). a) (top) Schematic representation for the experimental setup, (bottom) 5'-radiolabeled ssDNA EMSA with increasing concentrations of dLbCas12a-crRNA RNP first complexed with radiolabeled ssDNA before the addition of AcrVA4 and a complementary NTS (0.12 nM, left) or a non-complementary NTS (0.12 nM, right), **b)** (top) Schematic representation for the experimental setup, (bottom) 5'-radiolabeled dsDNA EMSA with increasing concentrations of dLbCas12a-crRNA first RNP complexed with radiolabeled bubbled dsDNA before the addition of AcrVA4, **c)** Experimental set up as in panel (a), 5'-radiolabeled ssDNA EMSA with increasing concentrations of dLbCas12a-crRNA RNP first complexed with a radiolabeled ssDNA before the addition of AcrVA4 and a mismatched NTS (0.12 nM), **d)** Experimental set up as in panel (b), 5'-radiolabeled dsDNA EMSA with increasing concentrations of dLbCas12a-crRNA first complexed with radiolabeled dsDNA before the addition of no competitor (left) or AcrVA4 (right). In all panels the bound and unbound fractions are indicated with black triangles.
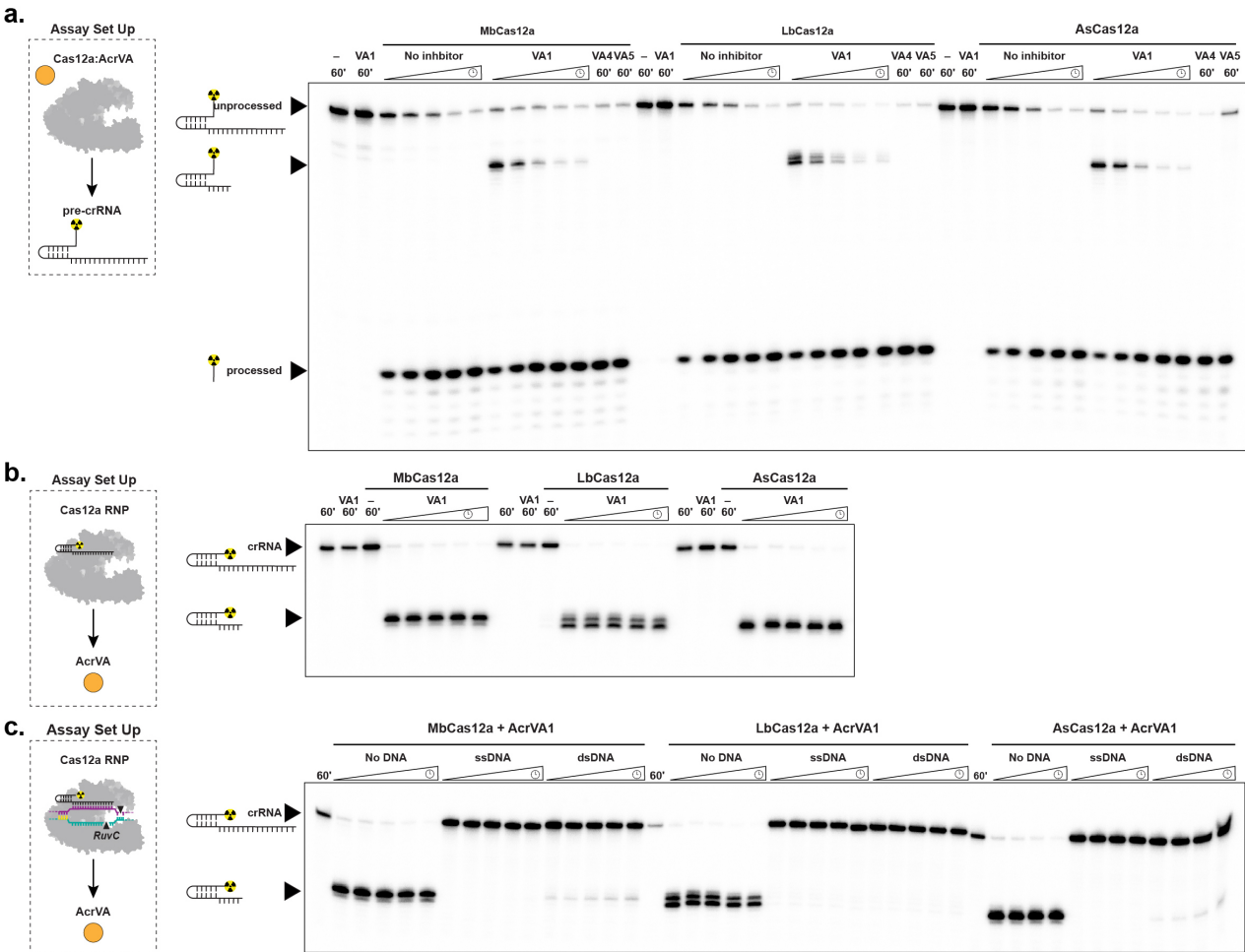
Extended Data Fig. 8 – AcrVA1 has no effect on pre-crRNA processing, truncates a Cas12a crRNA, but cannot mediate crRNA truncation on a Cas12a-crRNA-ss/dsDNA complex. a) 5'-radiolabeled kinetic pre-crRNA processing assays for (left to right) MbCas12a, LbCas12a, and AsCas12a complexed with or without AcrVAs. **b)** 5'-radiolabeled crRNA cleavage for (left to right) MbCas12a, LbCas12a, and AsCas12a first complexed with radiolabeled mature crRNA before addition of AcrVA1. **c)** 5'-radiolabeled crRNA cleavage for (left to right) MbCas12a-crRNA, LbCas12a-crRNA, and AsCas12a-crRNA pre-formed RNP first complexed target ssDNA or dsDNA (1 μM) before the addition of AcrVA1. Black triangles indicate the full-length crRNA, truncated crRNA, or pre-crRNA processed 5'-fragment. Time courses represent 1, 2, 5, 15, and 60 min.
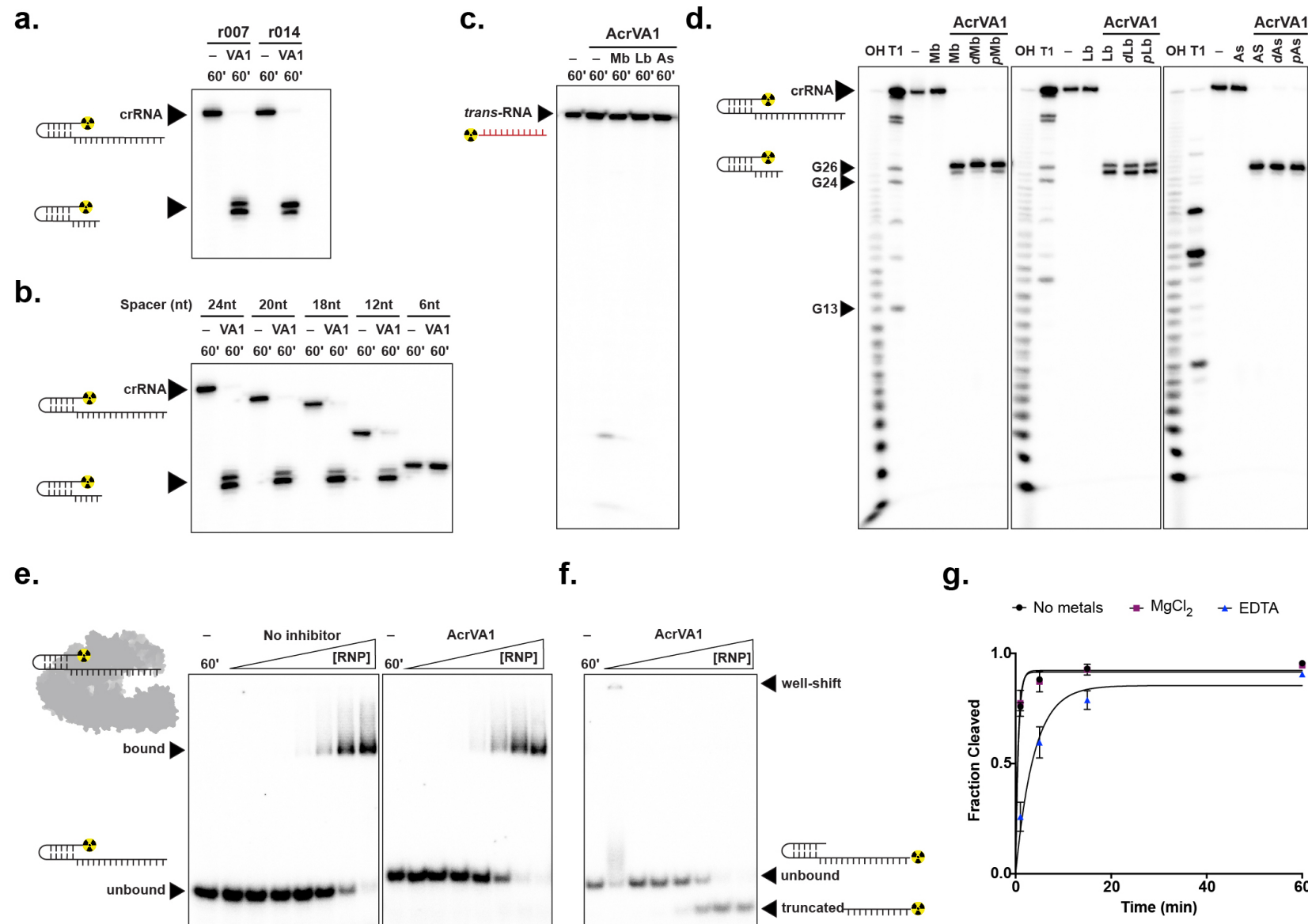
Extended Data Fig. 9 – Biochemistry of AcrVA1-triggered spacer truncation. a) 5'-radiolabeled crRNA cleavage in the presence of LbCas12a and AcrVA1 for two different crRNA spacer sequences demonstrating that AcrVA1-triggered spacer truncation is spacer sequence independent, **b)** 5'-

155 radiolabeled crRNA cleavage in the presence of LbCas12a and AcrVA1 for five different spacer lengths demonstrating that AcrVA1-triggered spacer
156 truncation requires a spacer greater than 6-nt in length, **c)** Radiolabeled *trans*-ssRNA cleavage after 60 minutes with (left to right) MbCas12a,
157 LbCas12a, and AsCas12a in the presence of AcrVA1 demonstrating no *trans*-ssRNA cleavage activity, **d)** 5'-radiolabeled crRNA cleavage assays with
158 Cas12a-crRNA orthologs complexed without or with AcrVA1 (full-length gel of Fig. 4c). For a single gel, treatments in the absence of AcrVA1 are
159 (left to right) crRNA hydrolysis ladder (OH), crRNA RNase T1 digestion (T1), untreated crRNA (-), and crRNA incubated with Cas12a (Mb/Lb/As).
160 Treatments in the presence of AcrVA1 are (left to right) wild-type Cas12a (Mb/Lb/As), dCas12a (D864A, dMb; D832A, dLb; D908A, dAs), and
161 processing dead Cas12a (K825A, pMb; K785A, pLb; K860A, pAs). A large black triangle indicates the full-length crRNA, smaller triangles indicate
162 the positions of mapped G-nucleotides for the LbCas12a crRNA, **e)** 5'-radiolabeled crRNA binding to LbCas12a shown by EMSA in the absence or
163 presence of AcrVA1. (left) LbCas12a binding to mature crRNA, (middle) LbCas12a binding to mature crRNA in the presence of AcrVA1, **f)** 3'-
164 radiolabeled crRNA binding to LbCas12a in the presence of AcrVA1 shown by EMSA. The bound, unbound, or AcrVA1 truncated fractions are
165 indicated with black triangles. **g)** Quantified 5'-radiolabeled LbCas12a-crRNA cleavage assay in the presence of LbCas12a and AcrVA1 where the the
166 cleavage buffer is supplemented with 0 mM or 5 mM $MgCl_2$, or 25 mM EDTA. Experimental fits are shown as solid lines and the calculated pseudo-
167 first-order rate constants (k_{obs}) (mean ± sd, *n*=3) are $1.7 ± 0.1$ min^{-1}, $1.9 ± 0.2$ min^{-1}, and $0.25 ± 0.03$ min^{-1} for conditions containing 0 mM $MgCl_2$, 5
168 mM $MgCl_2$, or 25 mM EDTA, respectively.
169
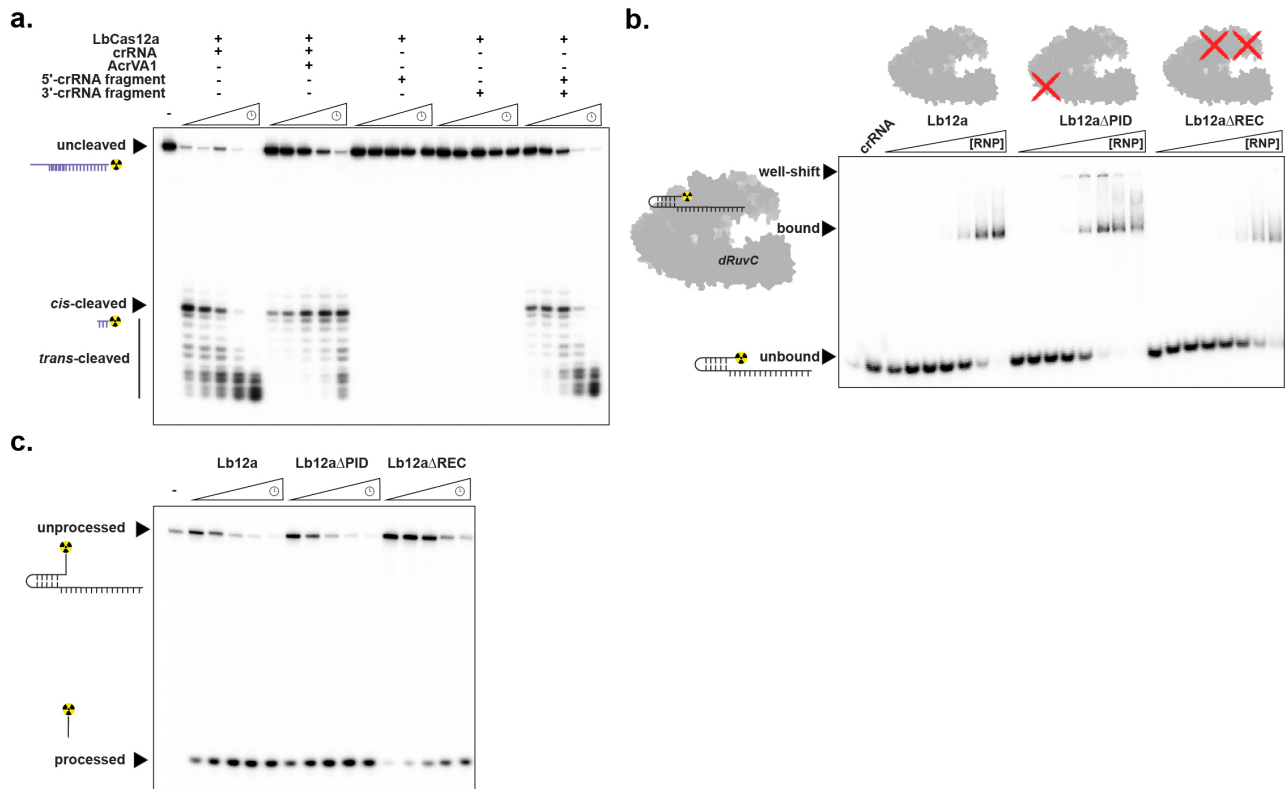
Extended Data Fig. 10 – Effect of domain truncations on crRNA binding/pre-crRNA processing and ssDNA-targeting by LbCas12a using crRNA fragments. a) 5'-radiolabeled kinetic ssDNA cleavage by (from left to right) LbCas12a in the presence of crRNA, crRNA and AcrVA1, the 5'-crRNA fragment, 3'-crRNA fragment, or both the 5'- and 3'-crRNA fragments. Time courses represent 1, 2, 5, 15, and 60 min. The uncleaved and *cis*-cleaved fractions are indicated with black triangles and the *trans*-cleavage products are indicated by a black bar. **b)** 5'-radiolabeled crRNA EMSA with increasing concentrations of LbCas12a complexed with radiolabeled crRNA. The bound and unbound fractions are indicated with black triangles, **c)** 5'-radiolabeled kinetic pre-crRNA processing assays for LbCas12a truncations. Time courses represent 1, 2, 5, 15, and 60 min. Black triangles indicate the full-length pre-crRNA, truncated pre-crRNA, or processed crRNA.